GEOLOGICAL CONSTRAINTS ON THE PRECAMBRIAN HISTORY OF EARTH'S ROTATION AND THE MOON'S ORBIT

George E. Williams
Department of Geology and Geophysics
University of Adelaide, Adelaide
South Australia, Australia

Abstract. Over the past decade the analysis of sedimentary cyclic rhythmites of tidal origin, i.e., stacked thin beds or laminae usually of sandstone, siltstone, and mudstone that display periodic variations in thickness reflecting a strong tidal influence on sedimentation, has provided information on Earth's paleorotation and the evolving lunar orbit for Precambrian time (before 540 Ma). Depositional environments of tidal rhythmites range from estuarine to tidal delta, with a wave-protected, distal ebb tidal delta setting being particularly favorable for the deposition and preservation of long, detailed rhythmite records. The potential sediment load of nearshore tidal currents and the effectiveness of the tide as an agent of sediment entrainment and deposition are related directly to tidal range (or maximum tidal height) and consequent current speed. Hence the thickness of successive laminae deposited by tidal currents can be a proxy tidal record, with paleotidal and paleorotational values being determined by analysis of measured records of lamina and cycle thickness. The validity of the findings can be investigated by testing the primary, observed values for internal self-consistency through application of the laws of celestial mechanics. Paleotidal and paleorotational values provided by late Neoproterozoic (~620 Ma) tidal rhythmites in South Australia are validated by these tests and indicate 13.1 ± 0.1 synodic (lunar) months/yr, 400 ± 7 solar days/yr, a length of day of 21.9 ± 0.4 h, and a relative Earth-Moon distance a/a_0 of 0.965 ± 0.005. The mean rate of lunar recession since that time is 2.17 ± 0.31 cm/yr, which is little more than half the present rate of lunar recession of 3.82 ± 0.07 cm/yr obtained by lunar laser ranging. The late Neoproterozoic data militate against significant overall change in Earth's moment of inertia and radius at least since 620 Ma. Cyclicity displayed by Paleoproterozoic (2450 Ma) banded iron formation in Western Australia may record tidal influences on the discharge and/or dispersal of submarine hydrothermal plumes and suggests 14.5 ± 0.5 synodic months/yr and $a/a_0 = 0.906 \pm 0.029$. The combined rhythmite data give a mean rate of lunar recession of 1.24 ± 0.71 cm/yr during most of the Proterozoic (2450–620 Ma), suggesting that a close approach of the Moon did not occur during earlier time. Concentrated study of Precambrian tidal rhythmites promises to illuminate the evolving dynamics of the early Earth-Moon system and may permit the lunar orbit to be traced back to near the time of the Moon's origin.

1. INTRODUCTION

The renowned German philosopher Immanuel Kant, in an article published in 1754 entitled "Examination of the question whether the Earth has undergone an alteration of its axial rotation," was the first to suggest that the motion of ocean tides raised mainly by the Moon and also by the Sun exerts a force on continental margins and the seafloor that slowly retards Earth's rotation [*Hastie*, 1900]. Kant believed that the retardation of Earth's rotation "must become infallibly perceptible through long periods" and that "the evidence of history might justly be adduced to give support to this hypothesis" [*Hastie*, 1900, p. 9]. However, he could find no historical evidence that the year formerly contained more days than it does now, and so he would "leave to others the merit of completing the subject by supplying this want when possible" [*Hastie*, 1900, p. 9]. Laplace rejected Kant's hypothesis of a slowly despinning Earth because it implied an apparent acceleration, as yet unobserved, also in the motion of the Sun and planets, and Kant's idea was otherwise largely ignored until the mid-nineteenth century. *Delaunay* [1865] revived Kant's hypothesis and showed that tidal friction may explain an acceleration of the Moon measured with respect to Earth's rotational timescale. Further contributions by J. C. Adams, W. Ferrel, W. Thomson (Kelvin) and P. G. Tait, G. H. Darwin, P. H. Cowell, H. Jeffreys, and others led to an improved theory of lunar-solar tidal friction based on Kant's fertile idea. An important part of this theory holds that the torque resulting from the Moon's attraction on Earth's tidal bulge transfers energy and angular
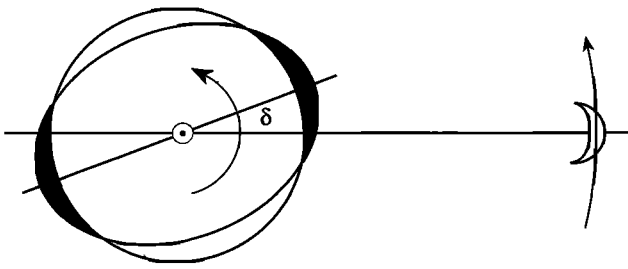
Figure 1. Diagram illustrating lunar tidal friction. The gravitational force of the Moon raises a tidal bulge in the solid Earth and oceans. Because of friction there is a delay in Earth's response, causing the tidal bulge to lead the Earth-Moon axis by a small angle δ. The Moon exerts a torque on the tidal bulge that retards Earth's rotation, thereby increasing the length of day. The torque that Earth's tidal bulge exerts on the Moon leads to an acceleration of the Moon's orbital motion, causing the Moon to recede from Earth [after *MacDonald*, 1964; *Lambeck*, 1980; *Wahr*, 1988].

momentum from Earth's rotation to the Moon's orbital motion, resulting in the slowing of Earth's rotation and the recession of the Moon (Figure 1). The solar torque also retards Earth's rotation, *Lambeck* [1980] giving the present ratio of solar to lunar torques as 1/4.6. The history of the theory of lunar-solar tidal friction is further discussed by *Berry* [1898], *Munk and MacDonald* [1960], *MacDonald* [1964], *Munk* [1968], and *Lambeck* [1980].

Tracing the history of Earth's tidal deceleration and

the evolution of the Moon's orbit is a major challenge for geology. The implications of employing the present rate of tidal energy dissipation on a geological timescale are catastrophic: Around 1500 Ma the Moon would have been close to Earth, with the consequence that the much larger tidal forces would have disrupted the Moon or caused the total melting of Earth's mantle and of the Moon [*Lambeck*, 1980]. No evidence exists for such cataclysmic events at that time. Moreover, the occurrence of sedimentary structures indicative of tidal deposition in Archean sandstones, mudstones, and carbonate rocks [*Eriksson*, 1977; *von Brunn and Mason*, 1977; *Watchorn*, 1980] is consistent with the presence of lunar tides at 3200–3000 Ma.

Wells [1963] provided a methodology for estimating the number of days per year in the geological past through his study of growth increments in recent and fossil corals. Counts of presumed daily growth lines between prominent bands, interpreted as annual, in Middle Devonian (380 Ma) corals suggested to Wells that there were ~400 daily growth lines (range 385–410) per year. Subsequent studies of skeletal growth increments in marine invertebrate fossils (corals, bivalves, and brachiopods) in general indicated an increasing number of synodic months per year, solar days per year (Figure 2), and solar days per synodic month going back to ~500 Ma, consistent with the hypothesis of lunar-solar tidal friction [*Rosenberg and Runcorn*, 1975]. (Synodic tides result from the interaction or beating of lunar and solar tides. The synodic or lunar month is the
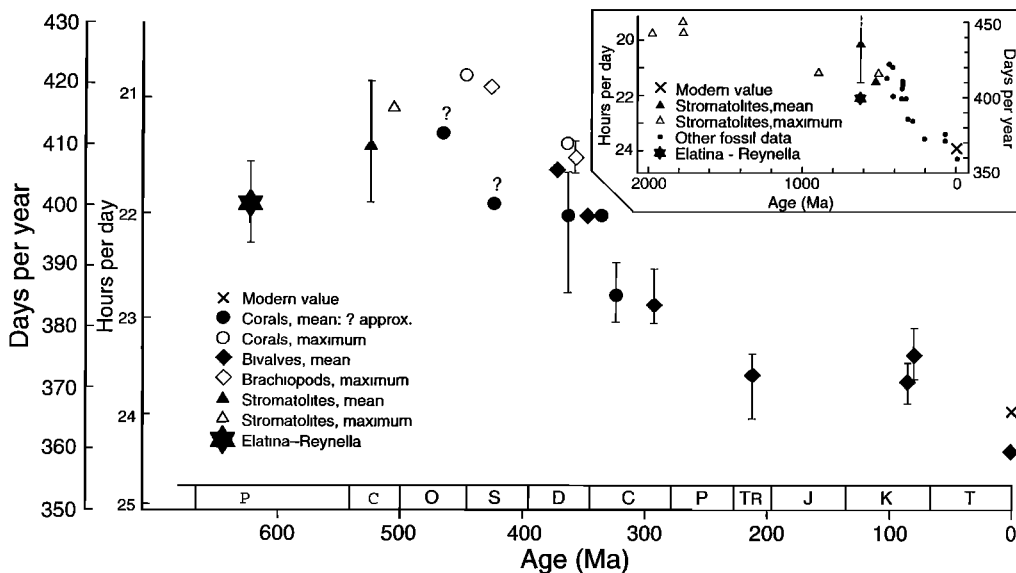
Figure 2. Plot of presumed solar days per year and length of day compiled from paleontological data: Phanerozoic data from *Scrutton* [1978] with available errors and additional data from *Berry and Barker* [1968], *McGugan* [1968], *Wells* [1970], *Mazzullo* [1971], *Pannella* [1972a, b], and *Vanyo and Awramik* [1985]. The datum for the late Neoproterozoic Elatina-Reynella tidal rhythmites (Table 1, column 6) also is shown. Abbreviations: P, Precambrian; Є, Cambrian; O, Ordovician; S, Silurian; D, Devonian; C, Carboniferous; P, Permian; TR, Triassic; J, Jurassic; K, Cretaceous; and T, Tertiary. The base of the Cambrian is shown at 540 Ma. Modified from *Williams* [1989c] and reproduced with the permission of the International Union of Geological Sciences.

interval between the same phases of the Moon, as from new Moon to new Moon, and the synodic fortnight is exemplified by the interval from opposition to conjunction or from conjunction to opposition of the Moon and the Sun, i.e., the interval between successive alignments of Earth, the Moon, and the Sun.)

The great hopes held for paleontological "clocks" have not, however, been fully realized. The Paleozoic data, if taken at face value, imply little overall change in the rate of tidal energy dissipation over the past ~500 Myr. Sustaining that high rate of dissipation implies a catastrophic close approach of the Moon near 2000 Ma [*Lambeck*, 1980], so raising doubts about the reliability of much paleontological data. According to paleontologist *Scrutton* [1978, p. 182] the common assumption that the growth increments in marine invertebrate fossils record the solar day and the synodic month may not be justified "because of earlier misunderstanding of the interplay between lunar and solar day stimuli and the effects of tide type" (the "lunar day" is the daily or diurnal lunar-solar tidal period, now 24.8 hours, resulting mainly from the lunar tide). *Scrutton* [1978, p. 182] concluded that the paleotidal and paleorotational values obtained from fossils "should be treated as approximations rather than as precise quantities for mathematical analysis." *Lambeck* [1980] and *Crisp* [1989] further questioned the validity of much of the data for Paleozoic marine invertebrates, suggesting that measurements may be biased toward expected results. The reliability of paleorotational data based on the growth patterns of Precambrian (before 540 Ma) stromatolites, laminated biosedimentary structures resulting from the sediment trapping and chemical action of algae [*Walter*, 1976], also has been challenged [*Hofmann*, 1973; *Lambeck*, 1980]. Because of these difficulties the study of paleontological clocks has made little progress in the last two decades.

Since the late 1980s the study of "cyclic rhythmites" of tidal origin [*Williams*, 1989c], i.e., vertically accreted thin beds or laminae usually of fine-grained sandstone, siltstone, and mudstone that display periodic variations in thickness reflecting a strong tidal influence on sedimentation, has provided a new methodology for the paleogeophysical analysis of Earth's rotation and the Moon's orbit that is applicable to the Precambrian. Cyclic tidal rhythmites can record periods that are ascribable to tidal pattern and type, thus avoiding some of the uncertainties associated with paleontological data. For example, diurnal laminae identified in tidal rhythmites are related to the lunar day, and synodic tides can leave a distinctive imprint in the rhythmite record (see section 3.1). Furthermore, rhythmite records may span several decades, revealing long-term paleotidal periods not readily seen in fossils.

This paper discusses the deposition of cyclic tidal rhythmites and the time series analysis of their encoded periods, emphasizes the geophysical implications of the paleotidal data, and shows how the study of tidal rhythmites can provide the past length of day (l.o.d.) and

eventually may permit the accurate tracing of the lunar orbit to near the time of the Moon's origin.
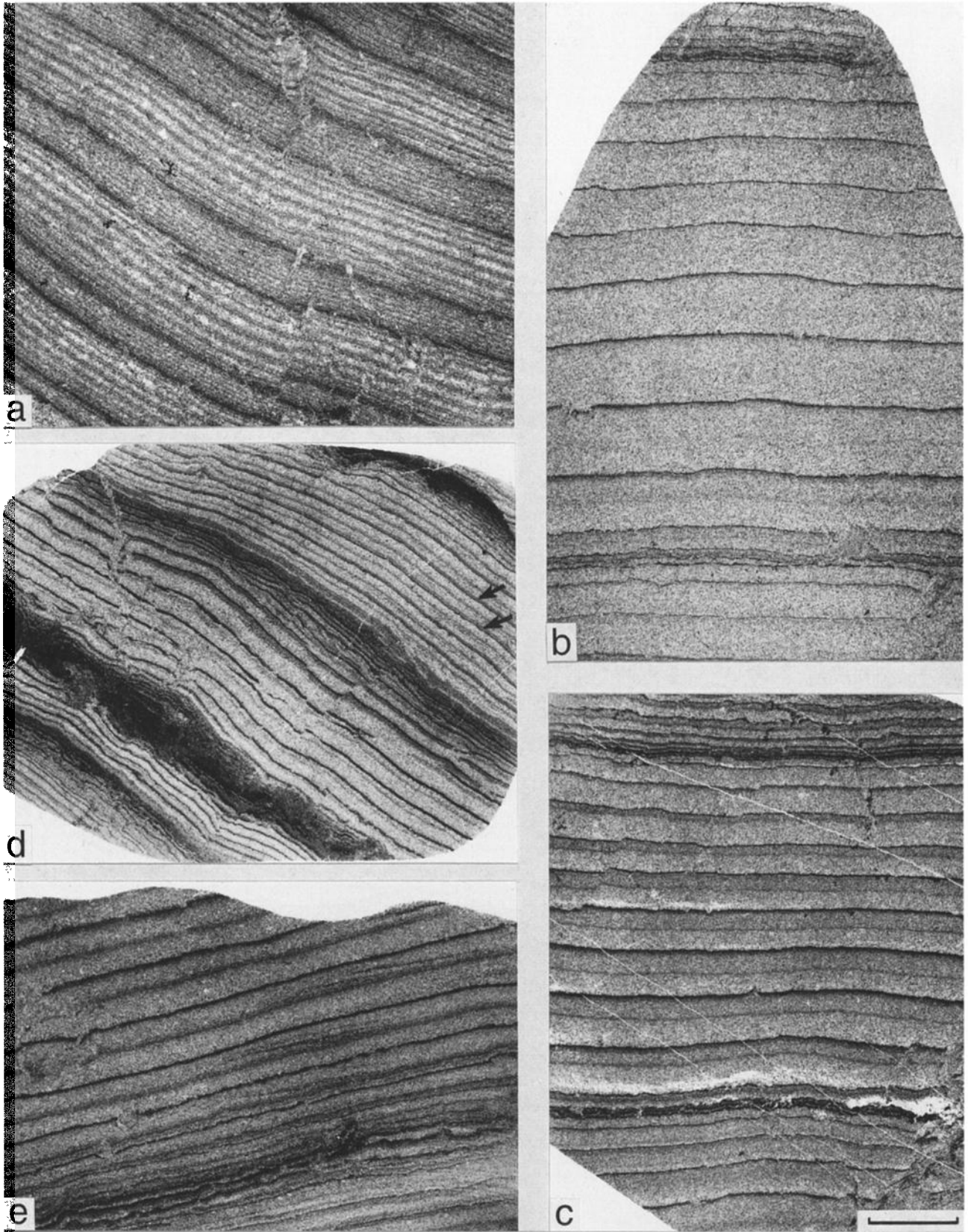
2. CYCLIC TIDAL RHYTHMITES

2.1. Deposition

Cyclic tidal rhythmites occur in modern marginal marine deposits [e.g., *Smith et al.*, 1990; *Dalrymple et al.*, 1991; *Tessier*, 1993], and comparable cyclic rhythmites (Figures 3 and 4) interpreted as tidal in origin have been identified in Neoproterozoic (1000–540 Ma) strata [*Williams*, 1989a, b, c, 1991; *Deynoux et al.*, 1993; *Chan et al.*, 1994] and in Phanerozoic (after 540 Ma) deposits [see *Smith et al.*, 1991]. Environments of deposition range from estuarine to upper and lower delta slope and distal, offshore tidal delta. A wave-protected, distal ebb tidal delta setting (Figure 5) may particularly favor the deposition and preservation of long, detailed rhythmite records. In this setting the flood tides converge radially toward the tidal inlet. There, fine-grained sandy, silty, and muddy sediment is entrained by semidiurnal and/or diurnal ebb tidal currents and transported mainly in suspension by turbid ebb tidal currents, plumes, or jets [*Özsoy*, 1986] via the main ebb channel to deeper water offshore, where the suspended sediment settles to form graded (upward fining) laminae (Figure 5, lower inset). Muddy caps may be deposited on the sandy laminae during slack water between tides. The potential sediment load of ebb tidal currents and the effectiveness of the tide as an agent of sediment entrainment and deposition are related directly to tidal range (or maximum tidal height) and consequent current speed [*FitzGerald and Nummedal*, 1983; *Boothroyd*, 1985].

Hence the thickness of successive laminae deposited on a distal ebb tidal delta can be a proxy tidal record. For example, thicker semidiurnal and diurnal sandy increments reflect the larger tidal ranges (or greater tidal heights) and faster ebb tidal currents that occur during the spring phase of the fortnightly tidal cycle when the Moon and the Sun are in conjunction and opposition. The quieter waters associated with the small tidal ranges at times of neap tides near quadrature (midway between conjunction and opposition of the Moon and the Sun) allow the settling of additional muddy material and the deposition of conspicuous mud bands or "mud drapes" that bound fortnightly groups of sandy and silty laminae, termed "neap-spring cycles." Each neap-spring cycle may contain up to 28 or more sandy or silty increments. Longer tidal cycles are recorded by systematic changes in the thickness of successive neap-spring cycles.

The sediment deposited in the distal, offshore setting is relatively undisturbed by the weak flood tide currents [*Özsoy*, 1986]. Preservation of the laminae deposited there would be enhanced by low wave energy and relatively rapid deepening beyond the terminal lobe of the ebb tidal delta. Such vertically accreted cyclic rhythmites represent the distal complement of laterally accreted,

cyclic tidal "bundle" deposits of cross-bedded sand bounded by mud drapes (Figure 5, top inset) observed in migrating sandbars in modern and subrecent tidal settings [*Visser*, 1980; *Boersma and Terwindt*, 1981; *Nio and Yang*, 1991].

Cyclic tidal rhythmites can accurately encode tidal periods at sites where deposition is continuous. However, because movement of sediment by tides may cease below a threshold tidal range and current speed [*Allen*, 1982; *FitzGerald and Nummedal*, 1983], a tidal sedimentary system can act as a filter, and in that circumstance a rhythmite record may include modulated or corrupted tidal periods:

1. A tidal sedimentary system will filter out the effects of the lesser semidiurnal constituent of the diurnal inequality (the unequal amplitude of successive semidiurnal tidal cycles) where tidal currents associated with the lesser constituent are too weak to transport sediment to the site of deposition [*de Boer et al.*, 1989; *Williams*, 1989c]. In this way, semidiurnal and mixed semidiurnal-diurnal tidal regimes can produce apparent diurnal patterns in rhythmite records.

2. Pauses in the deposition of sandy and silty laminae in the distal, offshore setting can occur around times of neap tides when tidal ranges and current speeds are minimal. Hence tidal rhythmite records of diurnal and semidiurnal increment thickness commonly are incomplete because of gaps in the record near neaps.

The development of tidal estuaries and inlets that are suitable for the generation of cyclic tidal rhythmites would be favored by the drowning of coastal rivers, valleys, and fjords through the global glacioeustatic rise of sea level that accompanies the retreat of ice sheets.

Hence favorable environments for the deposition of tidal rhythmites should have been common in postglacial, Holocene time (<10,000 years ago) and should be widespread today. Modern examples of such settings where tidal rhythmites are accumulating include Mont-Saint-Michel Bay, France [*Tessier*, 1993], the Bay of Fundy, Nova Scotia [*Dalrymple et al.*, 1991], and Glacier Bay, Alaska [*Smith et al.*, 1990]. Laminae deposited in a trap at the latter locality were assignable to diurnal and fortnightly tidal data. Neap-spring cycles also have been reported in a late Holocene (3665 years ago) tidal channel fill in the Netherlands [*Roep*, 1991]. The late Neoproterozoic Elatina-Reynella cyclic rhythmites in South Australia that are interpreted as tidal in origin (see section 2.2) occur within a glacial succession and may be related to sea level highstand [*Williams*, 1989a, c, 1991]. Furthermore, Pennsylvanian (Late Carboniferous) estuarine deposits in the eastern United States that display cyclic rhythmites also regarded as tidal in origin [e.g., *Kuecher et al.*, 1990; *Martino and Sanderson*, 1993] are coeval with Late Carboniferous glaciation of the southern supercontinent of Gondwanaland [see *Hambrey and Harland*, 1981] and likewise may be related to glacio-eustatic rise of sea level.

2.2. Recognition of Tidal Origin

To establish a tidal origin for ancient cyclic rhythmites, sedimentary features displayed by the rhythmites and closely associated strata should match features characteristic of tidal deposition that are observed in modern tidal deposits and rhythmites. Cyclic rhythmites are particularly well preserved in late Neoproterozoic (~620 Ma) strata in the Adelaide fold belt (Adelaide Geosyncline) near Adelaide and in the Flinders Ranges, South Australia. These deposits, termed the Reynella and Elatina rhythmites, respectively, display sedimentary features that indicate a tidal origin:

1. The Reynella rhythmites are associated with sandstone strata showing "herringbone cross-bedding" that comprises successive sets of cross-beds dipping in opposite directions, with the sets separated by a mud layer [*Williams*, 1989c, 1991]. This sedimentary structure records the opposite directions of sediment transport during successive ebb and flood tides and is typical of tidal environments [*Reineck and Singh*, 1973; *Reading*, 1978].

2. The Reynella rhythmites commonly display laminae that consist of "sublaminae" of unequal thickness (Figure 3; *Williams* [1989a, b, c, 1991]), and the same feature is displayed in parts of the Elatina rhythmites [*Williams*, 1991]. Such systematic alternation of relatively thick and thin laminae is observed in modern tidal deposits and uniquely records the diurnal inequality of the tides through its influence on the strength of successive semidiurnal tidal currents [*de Boer et al.*, 1989; *Dalrymple et al.*, 1991]. Hence the laminae and sublaminae in the Reynella and Elatina rhythmites are interpreted as diurnal and semidiurnal increments, respectively, of the lunar day. Failure to distinguish diurnal

---

Figure 3. (opposite) Thin sections of cyclic tidal rhythmites from the late Neoproterozoic Reynella Siltstone, South Australia, viewed with transmitted light; opaque muddy material appears darker than translucent sandy layers. Scale bar is 1 cm for all photographs. The rhythmites comprise weakly graded (upward fining) diurnal laminae and semidiurnal sublaminae of fine-grained sandstone with muddy tops, grouped in fortnightly neap-spring cycles; conspicuous mud drapes bounding the neap-spring cycles were deposited near times of neap tides. (a) Nine alternately thick and thin neap-spring cycles, indicating the monthly inequality of paleo-spring tides. (b) One complete neap-spring cycle containing diurnal laminae up to 8 mm thick. (c) One complete neap-spring cycle containing diurnal laminae up to 6 mm thick; semidiurnal sublaminae also are evident. (d) The uppermost neap-spring cycle comprises diurnal laminae up to 3 mm thick marked by alternate darker bands and semidiurnal sublaminae of about equal thickness; the arrows mark double mud drapes. In the neap-spring cycle immediately below, the lower semidiurnal sublamina in each pair is the thicker, indicating the diurnal inequality of paleotides. (e) Portions of two neap-spring cycles; in the upper part of the photograph, diurnal laminae up to 6 mm thick marked by alternate darker bands contain semidiurnal sublaminae of about equal thickness. Reproduced from *Williams* [1989a] with the permission of the Geological Society, London.
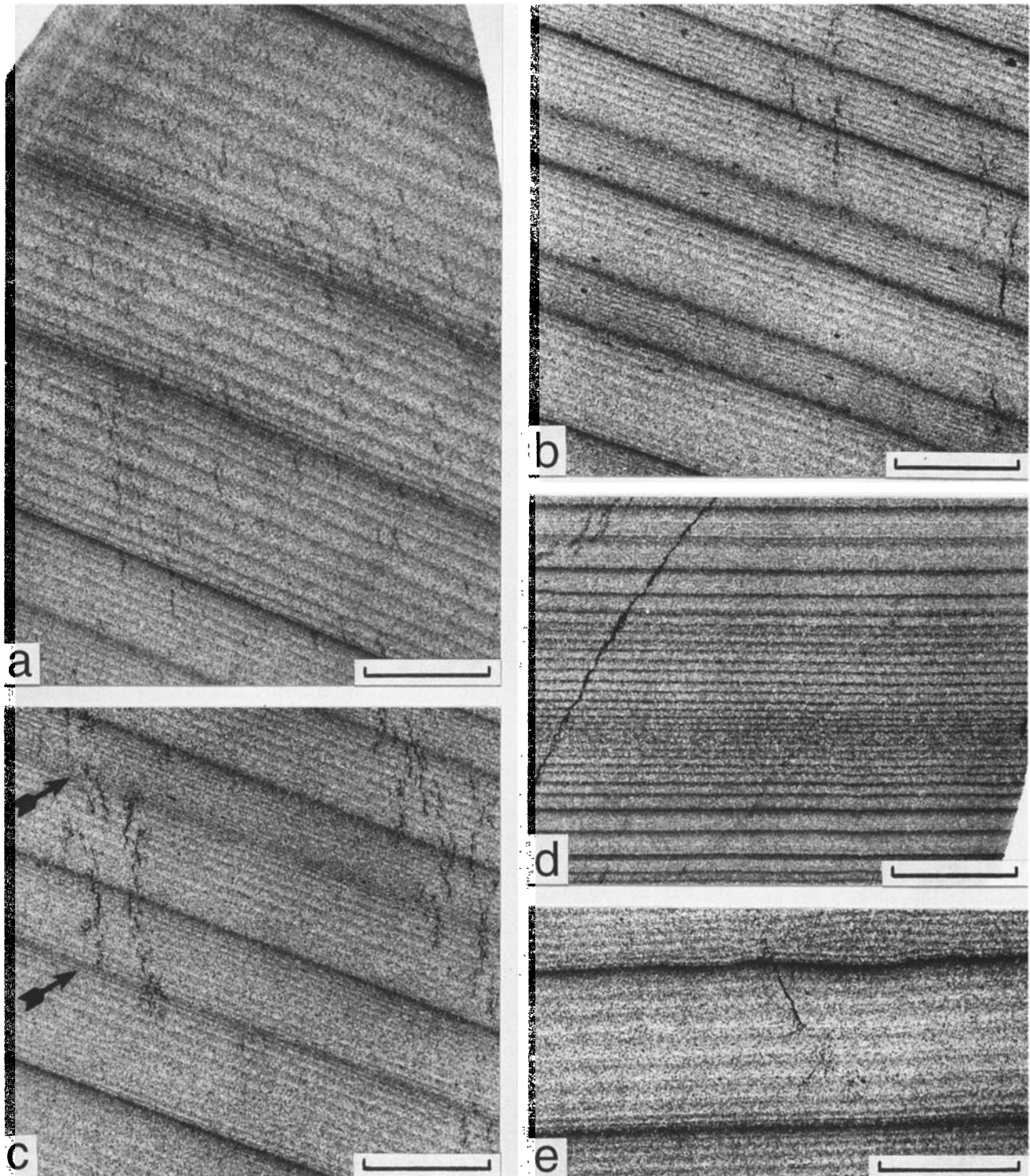
Figure 4. Thin sections of rhythmites from drill core of the late Neoproterozoic Elatina Formation, South Australia, viewed with transmitted light; opaque muddy material appears darker than translucent sandy and silty layers. Scale bars are 1 cm. (a) Four complete fortnightly neap-spring cycles of ~10–14 graded, diurnal laminae are bounded by conspicuous, dark, mud drapes deposited near times of neap tides. (b) Alternately thick and thin neap-spring cycles indicating the monthly inequality of paleo-spring tides. (c) Neap-spring cycles with alternate boundaries represented by very thin silty laminae (arrows) rather than mud drapes; such little abbreviated neap-spring cycles were deposited near solstices, when neap-tidal ranges were maximum (see section 3.1). (d) A group of thin (0.5–3.0 mm) neap-spring cycles representing just over 1 year's deposition; internal lamination between mud drapes is discernible only in a few places. (e) A neap-spring cycle comprising diurnal laminae as well as semidiurnal sublaminae. Reproduced from *Williams* [1991] with the permission of the Canadian Society of Petroleum Geologists, Calgary.
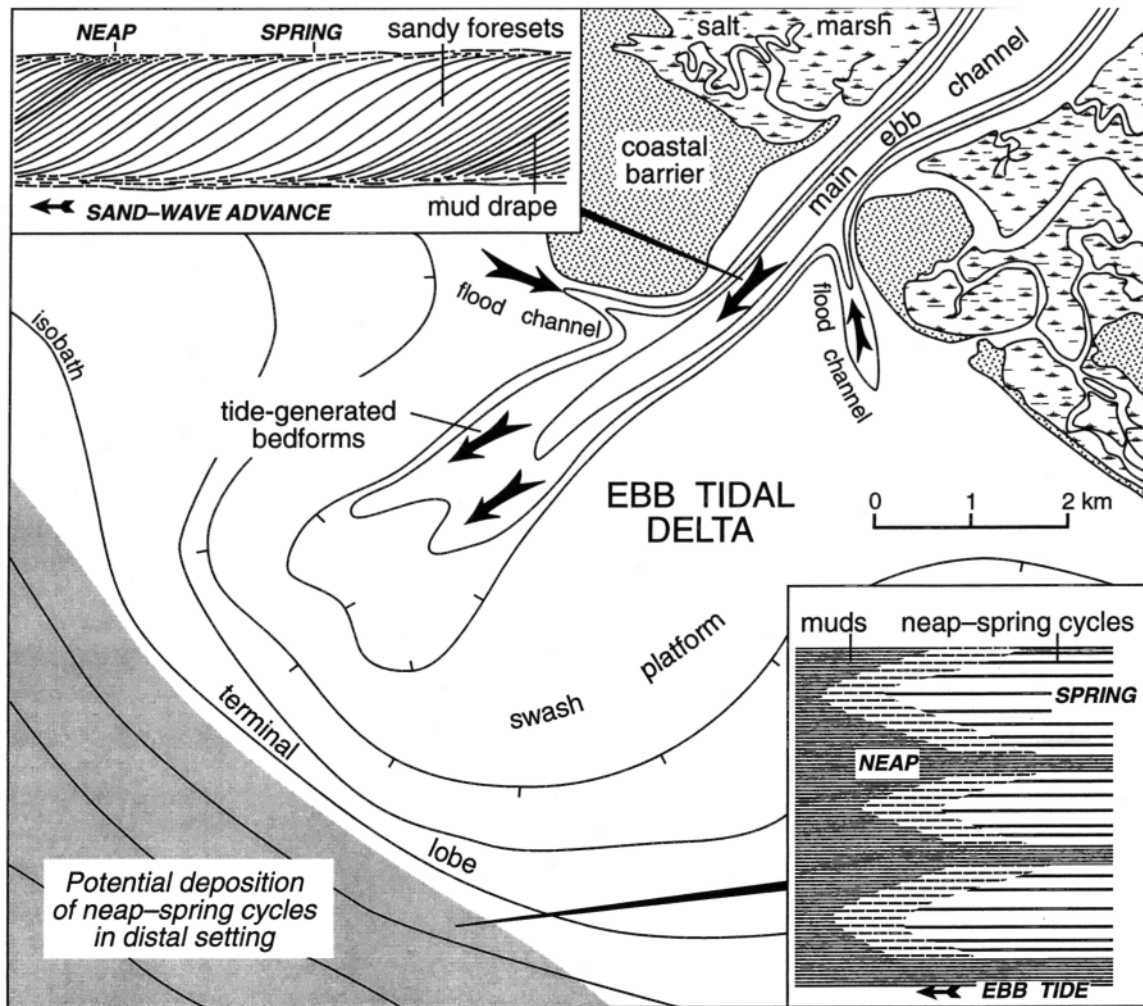
Figure 5. Envisaged environment of deposition for the Elatina-Reynella cyclic tidal rhythmites, employing a hypothetical ebb tidal delta adapted from *Imperato et al.* [1988]. The flood tides converge radially toward the tidal inlet, where fine-grained sediment is entrained by ebb tidal currents and transported mainly in suspension via the main ebb channel to deeper water offshore. There the suspended sediment settles to form neap-spring cycles of thin, graded laminae mostly of sand and silt (shown schematically in bottom inset). Farther offshore, the neap-spring cycles become progressively more abbreviated near positions of neap tides and eventually pass into marine shelf mud. Where protected from wave action, the distal ebb tidal delta setting favors the deposition and preservation of long rhythmite records. Tidal "bundle" deposits of cross-bedded sand (top inset) are confined to proximal, nearshore tidal channels. Modified from *Williams* [1989c] and reproduced with the permission of the International Union of Geological Sciences.

laminae and semidiurnal sublaminae in rhythmites could lead to the acquisition of inaccurate paleotidal data.

3. The Reynella and Elatina rhythmites display groups or cycles that comprise up to 16 sandy or silty diurnal laminae that are thicker near the center of each cycle and that are bounded by mud drapes (Figures 3 and 4). These cycles are comparable to the neap-spring cycles that occur in modern tidal deposits [*Smith et al.*, 1990; *Dalrymple et al.*, 1991; *Tessier*, 1993] and record the fortnightly tidal cycle.

The above observations, together with directional paleocurrent data and paleogeographic reconstruction for the Elatina Formation [*Preiss*, 1987; *Williams*, 1991], indicate that the Reynella and Elatina rhythmites were

deposited in distal ebb tidal settings (Figure 5) near the margin of a marine gulf. The adjacent hinterland was a periglacial desert blanketed by wind-blown sands and with no perennial rivers [*Williams*, 1998a]. The envisaged setting with few fluvial or other random events interfering with periodic tidal processes in the inlet or estuary is especially favorable for the deposition of cyclic tidal rhythmites.

The tidal interpretation of the Reynella and Elatina rhythmites is reinforced by the similarity of the rhythmite patterns to modern tidal records (section 2.3) and the determination of internally self-consistent paleotidal and paleorotational values through analysis of the rhythmite data (sections 3.1 and 3.2).

2.3. Interpretation and Analysis of Tidal Rhythmite Records

The Reynella Siltstone, a stratigraphic member of the Elatina Formation near Adelaide and part of the Marinoan glacial deposits in the southern Adelaide fold belt [*Preiss*, 1987], contains graded laminae of fine-grained sandstone and siltstone up to 2 cm thick that commonly have a thin muddy cap (Figure 3). The laminae are grouped in neap-spring cycles from 0.5 to >6 cm in thickness, with an alternation of relatively thick and thin cycles (Figure 3a) occurring in many places. Mud drapes commonly bound the neap-spring cycles (Figures 3a and 3d). However, mud drapes are thinner and less conspicuous for some of the thick cycles, which do not appear to be abbreviated near positions of neap tides and commonly contain 14–15 laminae (Figures 3b and 3c). As noted above, some of the laminae in these thick neap-spring cycles consist of two graded layers or sublaminae (Figures 3c, 3d, and 3e) that are interpreted as diurnal and semidiurnal increments, respectively, and which indicate a mixed semidiurnal-diurnal paleotidal pattern. Rarely, double mud drapes are associated with the sublaminae (Figure 3d), suggesting the influence of both semidiurnal ebb and flood tides.

The Elatina Formation in the northern Adelaide fold belt also is part of the late Neoproterozoic Marinoan glacial deposits and includes a 10-m-thick rhythmite unit that can be shown to represent >60 years of continuous tidal deposition [*Williams*, 1989a, c, 1991, 1998b]. This unit is penecontemporaneous with the Reynella rhythmites. The Elatina rhythmites (Figure 4) comprise graded laminae 0.2–3.0 mm thick of very fine grained sandstone and siltstone. Conspicuous neap-spring cycles up to 2 cm thick contain 8–16 laminae, which are interpreted as diurnal increments, with semidiurnal sublaminae occurring locally (Figure 4e; *Williams* [1991]). Evidently, the current speeds associated with the smaller semidiurnal tide usually were too low to permit the transport of sediment to the site of deposition. Further evidence of sedimentary modulation of tidal periods is provided by the relatively small number of diurnal laminae (as few as 8–10) in many of the Elatina neap-spring cycles, indicating that such cycles are abbreviated through nondeposition of sandy laminae around times of neap tides when mud drapes were laid down [*Williams*, 1989a, b, c, 1991]. At regular intervals, however, alternate mud drapes between neap-spring cycles are not well formed and are represented by very thin silty laminae (Figure 4c), and at these positions the neap-spring cycles appear largely unabbreviated. The rhythmites typically show an alternation of relatively thick and thin neap-spring cycles (Figures 4b and 4c). Thin (0.5–3.0 mm) neap-spring cycles (Figure 4d) that occur at the base of the rhythmite unit are interpreted as the most distal, offshore deposits that were buried by the seaward building tidal delta.

Long, continuous paleotidal records of sequential thickness measurements provide the most reliable pa-

leotidal periods and frequencies and are best exemplified by the Elatina 60-year record of neap-spring cycle thickness [*Williams*, 1989a, b, 1991]. Because outcrop of the Elatina rhythmites is poor, drill cores of the 10-m-thick rhythmite unit were obtained from three vertical holes drilled up to 200 m apart to allow construction of a complete rhythmite record. The composite log obtained from matching of the cores comprises a virtually unbroken paleotidal record of 1580 neap-spring cycles whose thicknesses were readily measured. In addition, a piece of core 93 cm long that contained well-preserved laminae was selected for the measurement of lamina thickness, which was done on photographic enlargements of thin sections of the core. This short paleotidal record comprises measurements of 1337 distinguishable diurnal laminae from 110 neap-spring cycles spanning 4.2 years. All thickness measurements were made with an increment measurer and have a precision of 0.01 mm.

Both the short and long Elatina records are conspicuously periodic over their entire lengths, and representative extracts from each record are shown in Figures 6a and 7 (other parts of these records are illustrated by *Williams* [1989a, b]). The thicknesses of neap-spring cycles and constituent diurnal laminae are directly related, the thickest cycles typically containing the thickest laminae. Representative plots for dominantly synodic tides at Townsville, Queensland, employing maximum tidal height as a relative measure of tidal range, are shown in Figures 6b and 8 for comparison with the Elatina patterns. (A 20-year tidal record for Townsville for 1966–1985 was provided for comparative study because of its completeness and synodic character.)

The patterns of the Elatina and Townsville records show strong similarities. Plots of diurnal lamina thickness (Figure 6a) are comparable to plots of daily tidal height (Figure 6b). Furthermore, regular changes in the thickness of neap-spring cycles (Figure 7) are similar to variations in fortnightly tidal height (Figure 8). Characteristically, the Elatina data show alternately thick and thin neap-spring cycles, and the Townsville data show fortnightly cycles of alternately high and low heights. This distinctive pattern reflects the "monthly inequality" of spring tidal heights and ranges resulting from the elliptical lunar orbit; relatively high spring tides are raised at perigee when the Moon is closest to Earth, and relatively low spring tides occur a fortnight later at apogee when the Moon is farthest from Earth.

Three additional extracts from the lower, middle, and upper parts of the long Elatina record are shown in Figure 9. The most conspicuous regular variation in the thickness of Elatina neap-spring cycles (Figures 7a, 7b, and 9) is marked by peaks whose spacing averages 26.2 ± 0.9 (error $\pm 1\sigma$ and range 23–28) neap-spring cycles. Sixty such peaks are present in the measured Elatina record. The peaks are equated with maxima in the height of spring tides at Townsville (Figures 8a and 8b), which mark the nontidal annual or seasonal oscillation of sea level [*Pariwono et al.*, 1986]. This global
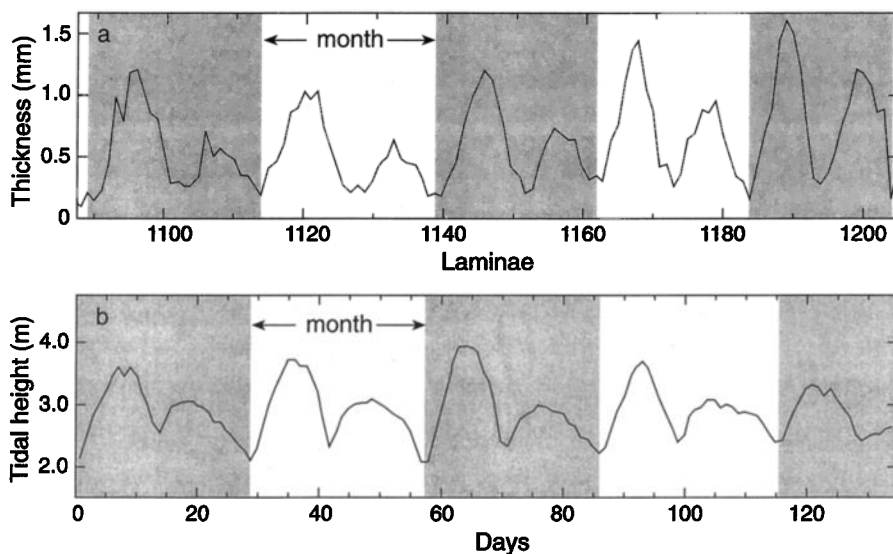
Figure 6. (a) Representative extract from the Elatina paleotidal record of diurnal lamina thickness, showing neap-spring cycles of alternately high and low maxima (lamina number increases up the stratigraphic succession). (b) Maximum daily tidal height from January 1 to May 14, 1966, for Townsville, Queensland, showing synodic fortnightly cycles of alternately high and low height reflecting the monthly inequality of spring tides caused by the elliptical lunar orbit. (The Townsville data comprise the two highest daily readings and were further smoothed by a three-point filter weighted 1, 2, 1.) Shaded and unshaded areas in Figures 6a and 6b are pairs of successive cycles representing the synodic month, although the neap-spring cycles in Figure 6a are abbreviated at lamina-thickness minima, which mark the positions of neap tides.

oscillation is caused by a complex interaction of physical processes including changes in atmospheric pressure, winds, and water temperature; in most places the highest sea level occurs in the autumn, with the oscillations in the Northern and Southern Hemispheres being out of phase [*Komar and Enfield*, 1987]. The periodicity of this sea level oscillation at a particular site thus reflects the solar year. The moderate variation in spacing of the annual signal in the Elatina record is consistent with a seasonal climatic effect. This cyclicity provides a time-scale that indicates that the Elatina record spans ~60 years.

Second-order peaks in the Townsville record of spring tidal height (Figure 8b) reflect the semiannual tidal cycle of the Sun's declination, which raises its highest spring tides around times of the autumnal and vernal equinoxes when the Sun is above the equator. Comparable second-order peaks that occur in the Elatina record of neap-spring cycle thickness (Figures 7b and 9) are ascribed to the semiannual tidal cycle. Alternate semiannual peaks in both the Townsville and Elatina records are obscured by the nontidal annual peaks, although in parts of the Elatina record the semiannual peak can be discerned as an asymmetry in the annual peak. The relative phases of the interpreted annual and semiannual signals in the Elatina rhythmites do not change significantly over the measured record.

Fourier spectral analysis of the Elatina 60-year record of neap-spring cycle thickness provides a virtually noise-free spectrum with sharp spectral peaks (Figure 10a),

consistent with the manifest periodic nature of the entire Elatina record and confirming that periodic processes dominated during deposition. This spectrum is compared to that for a 20-year record of height of spring tides at Townsville (Figure 10b), which shows annual, semiannual, and monthly peaks. The main peaks in the Elatina spectrum also indicate annual, semiannual, and monthly periods, although the two spectra show markedly different relative power for respective peaks, and the annual and semiannual periods in the Elatina spectrum differ from their modern counterparts.

The spectrum for the Elatina 4.2-year record of diurnal lamina thickness shows peaks at 333 and 159 diurnal laminae, representing the annual oscillation of sea level and the semiannual tidal cycle, respectively (Figure 10c). Because many of the Elatina neap-spring cycles are abbreviated at positions of neap tides, these peaks are shifted to higher frequencies. Support for such spectral shifts is provided by the occurrence of strong peaks at 11.0–12.5 diurnal laminae that represent neap-spring cycles, in contrast to direct counts of 14–15 diurnal laminae in apparently unabbreviated, thick neap-spring cycles in the coeval Reynella rhythmites. The numerous spectral peaks from 10.3 to 13.5 diurnal laminae (Figure 10c) do not indicate paleotidal periods because it can be shown that they result from periodic abbreviation of the Elatina record (see section 3.1). Claims to have determined the number of days per month by spectral analysis of the abbreviated Elatina record of diurnal lamina thickness [*Sonett et al.*, 1996a; *Sonett and Chan*, 1998] are
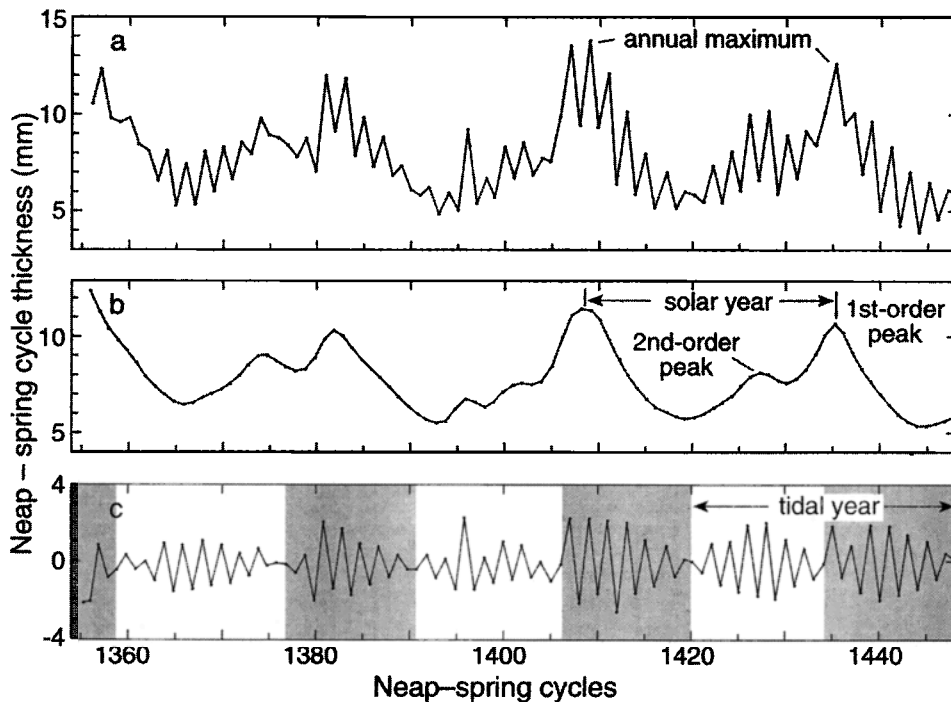
Figure 7. Representative extract from the Elatina paleotidal record of neap-spring cycle thickness (neap-spring cycle number increases up the stratigraphic succession). (a) Unsmoothed curve and (b) smoothed curve (five-point filter weighted 1, 4, 6, 4, 1), showing first-order peaks that are equated with the nontidal annual or seasonal maximum height of sea level and so define the solar year and second-order peaks that are interpreted as recording the semiannual tidal cycle. (c) Residual curve (curve in Figure 7a minus that in Figure 7b), showing the "tidal year" (see section 3.1 and Figure 12 for explanation). The boundaries between shaded and unshaded areas in Figure 7c mark 180° phase reversals in the sawtooth pattern; the latter is interpreted as reflecting the monthly inequality of spring tides.

unwarranted, as are the proposed dynamical implications, because the raw data are corrupted.

Confirmation that spectra for incomplete or short tidal records can be misleading is provided by the spectrum for a 2.8-year record of maximum daily height of sea level at Weipa, Queensland (Figure 10d), which has features in common with Figure 10c. The annual oscillation dominates sea level variation at Weipa, but in the spectrum the annual period is represented by a strong peak at 256 solar days, and peaks representing semiannual, monthly, and fortnightly periods also are shifted to higher frequencies.

Records of diurnal and semidiurnal increment thickness obtained from other tidal rhythmites commonly are incomplete because of pauses in the deposition of such increments near times of neap tides. Any abbreviation of the raw data must be recognized if paleotidal records and spectra are to be interpreted correctly. Potential difficulties in obtaining accurate paleotidal values by the analysis of tidal rhythmites are further discussed by *Kvale et al.* [1995]. Hence it is important to investigate, where possible, the self-consistency and geophysical validity of claimed paleotidal and paleorotational values (see section 3.2).

3. EARTH'S PRECAMBRIAN ROTATION

3.1. Neoproterozoic Tidal and Rotational Values

The Elatina and Reynella rhythmites together provide an unrivaled data set that comprises a full range of paleotidal and paleorotational values at ~620 Ma (Table 1, column 6). The derivation of these values is explained below. Values given in sidereal time (i.e., with reference to the fixed stars) are required for dynamical calculations in section 4.

Thick, apparently unabbreviated neap-spring cycles in the Reynella rhythmites (Figures 3b and 3c) contain 14–15 diurnal laminae, in agreement with the presence of up to 29 diurnal laminae in pairs of successive little abbreviated neap-spring cycles, recording the synodic month, in the Elatina rhythmites (Figure 4c). The counts for the Reynella and Elatina rhythmites suggest 29–30 lunar days per synodic month and thus imply 30.5 ± 0.5 solar days/synodic month.

The number of solar days per sidereal month, t, is given by

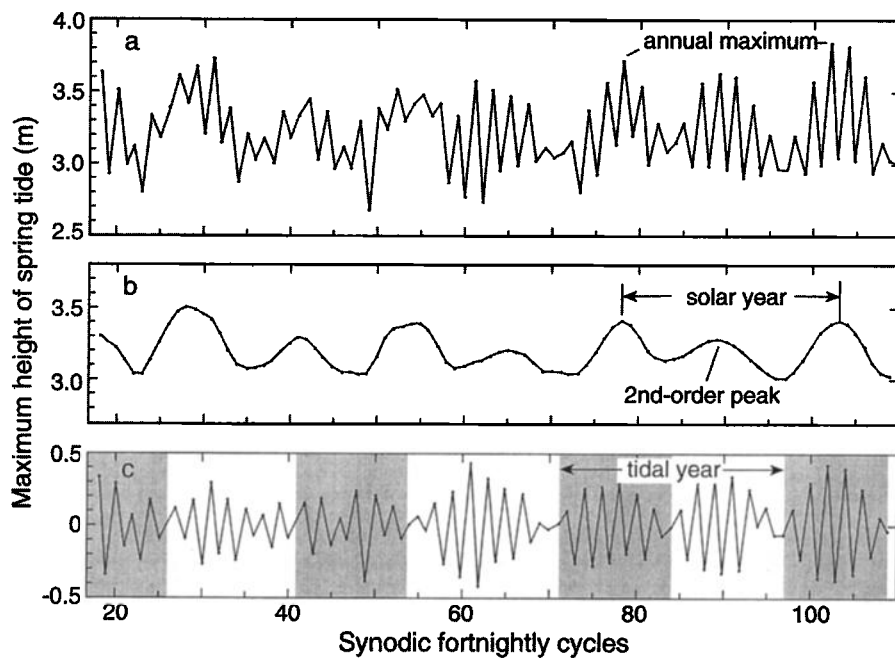$$t = \frac{t_L}{1 + \dfrac{t_L}{Y_D}}, \qquad (1)$$

Figure 8. Typical tidal patterns for Townsville. (a) Maximum height of synodic fortnightly tidal cycles (average of the two highest readings for each spring tidal cycle) from September 14, 1966, to June 3, 1970. (b) Smoothed curve (five-point filter weighted 1, 4, 6, 4, 1), showing first-order peaks that mark the nontidal annual or seasonal oscillation of sea level and so define the solar year and second-order peaks that reflect the semiannual tidal cycle. (c) Residual curve (curve in Figure 8a minus that in Figure 8b), showing the tidal year (see section 3.1 and Figure 12 for explanation). The boundaries between shaded and unshaded areas in Figure 8c mark 180° phase reversals in the sawtooth pattern; the latter reflects the monthly inequality of spring tides. Modified from *Williams* [1989a] and reproduced with the permission of the Geological Society, London.

where t_L is the number of solar days per synodic month and Y_D is number of solar days per year [after *Runcorn*, 1979]. Hence 30.5 ± 0.5 solar days/synodic month at ~620 Ma gives t = 28.3 ± 0.5 solar days.

Spectral analysis of the Elatina 60-year record indicates that the late Neoproterozoic year is represented by 26.1 or 26.2 (±0.2) neap-spring cycles, the precise figure obtained depending on the method of spectral analysis (Figure 10a and *Williams* [1989a, b]), and contained 13.1 ± 0.1 synodic months. Data for the coeval Reynella and Elatina rhythmites therefore indicate (30.5 ± 0.5) (13.1 ± 0.1) = 400 ± 7 solar days/yr and hence 21.9 ± 0.4 h/d at ~620 Ma, taking the length of the year at that time as not significantly different from the present length of 31.56 × 10⁶ s (see section 4).

The second harmonic of the annual cycle has a period of 13.1 neap-spring cycles and records the semiannual tidal cycle. This cycle, through its modulation of tidal range, influenced neap tidal pauses in the deposition of diurnal clastic laminae in the Elatina rhythmites, thereby modulating the number of laminae deposited per neap-spring cycle (Figure 11). The numerous spectral peaks from 10.3 to 13.5 diurnal laminae (Figure 10c) are explained by this "frequency modulation" and hence are products of the sedimentary system. The stratigraphic positions of neap-spring cycles that are bounded by very thin silty laminae rather than mud drapes, where neap-

spring cycles appear to be little abbreviated (Figure 4c), are at or near the semiannual peaks in the number of diurnal laminae per neap-spring cycle (continuous curve in Figure 11b). Evidently, the deposition of clastic laminae was not interrupted during semiannual maxima in tidal range at neaps, thereby causing the deposition of neap-spring cycles with the greatest number of diurnal laminae. By comparison with tidal data for Townsville and the Severn Estuary in England [*Allen*, 1990] and with the annual sea level oscillation, which usually gives the highest sea level in the autumn [*Komar and Enfield*, 1987], the positions of summer and winter solstices and autumnal and vernal equinoxes can be identified in the Elatina record (Figure 11b). The semiannual peaks in diurnal laminae per neap-spring cycle occurred near solstices, when neap tidal heights and ranges are greatest, and the high peaks in diurnal lamina thickness mark high sea level in the autumn.

Figure 12 confirms the synodic character of the Elatina paleotidal pattern. The dominantly synodic tides at Townsville display a distinctive variation in the height of successive fortnightly cycles (Figures 8c and 12b): (1) As explained in section 2.3, the elliptical lunar orbit produces fortnightly cycles of alternately high and low height (monthly inequality), plotting as a "sawtooth" pattern. (2) There is a regular modulation of the amplitude of the sawtooth pattern, with 180° changes in phase
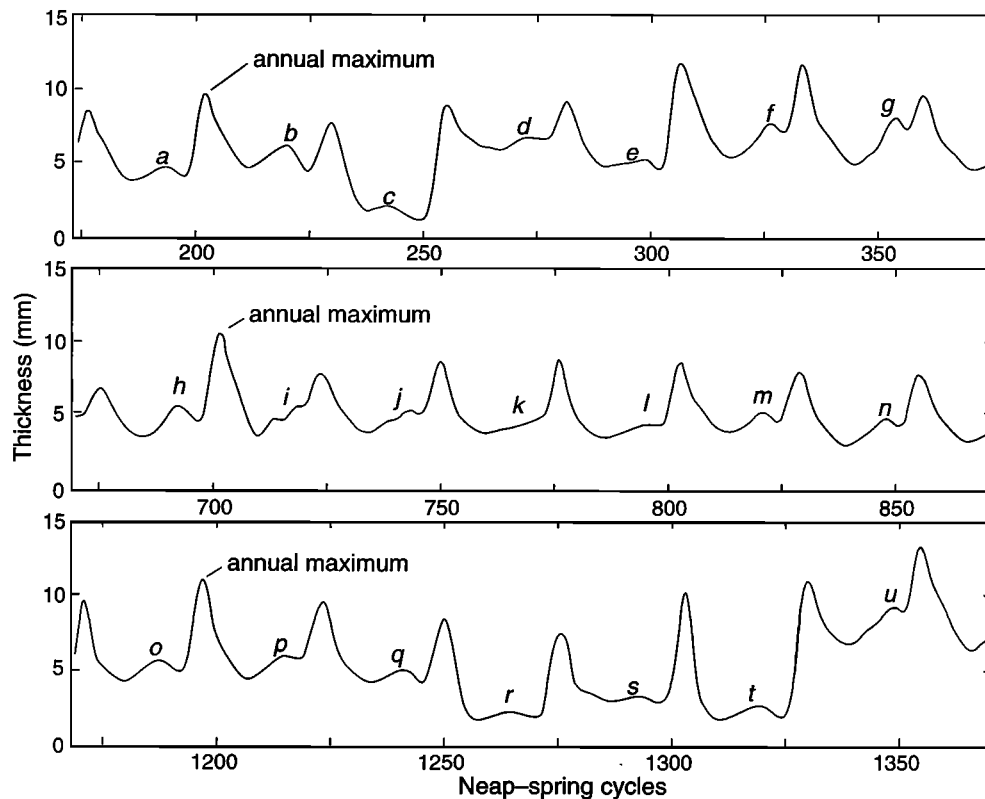
Figure 9. Three extracts from the Elatina paleotidal record of neap-spring cycle thickness (smoothed by a five-point filter weighted 1, 4, 6, 4, 1; neap-spring cycle number increases up the stratigraphic succession), showing 24 first-order peaks that are equated with the nontidal annual or seasonal maximum in sea level. The plots span the three intervals where the second-order peaks (peaks a–u), which are interpreted as reflecting the semiannual paleotidal cycle, show minimal height (peaks c–e, j–l, and q–t); the symmetry of the annual peaks tends to be greatest at these places. Over the 60-year record, a period of 19.5 ± 0.5 years is revealed by variation in the height of the semiannual peaks (see Figure 13a), as measured from the base of the preceding trough to the top of the peak or to the midpoint between rare twin peaks (peaks i and j). Neap-spring cycle thickness shows a gradual decrease for cycles 1200–1325 and abrupt increases at cycles 250 and 1325; these nonperiodic changes evidently reflect sedimentary processes on the tidal delta such as a gradual blocking of the main ebb channel followed by channel avulsion.

(i.e., a reversal in the order of high and low cycles) occurring when the amplitude of the sawtooth pattern is minimal.

Figures 12a and 12b show that maximum monthly inequality of spring tidal height occurs for successive conjunctions and oppositions of the Moon and the Sun when Earth, the Moon, and the Sun are aligned with the major axis of the elliptical lunar orbit. Minimum monthly inequality and 180° change in phase occur when all bodies are aligned normal to the major axis of the lunar orbit. The mean period for a full 360° change in phase, which could be termed the "tidal year," currently is 13.95 synodic months. This is longer than the present solar year of 12.37 synodic months because of the prograde rotation (i.e., in the same sense as Earth's revolution around the Sun) of the lunar perigee (Figure 12a). The Elatina record displays a comparable synodic pattern through an alternation of relatively thick and thin neap-spring cycles (Figures 7c and 12c). Spectral analy-

sis shows that the tidal year had a period of 14.6 ± 0.1 synodic months at ~620 Ma [*Williams*, 1989b, 1998b].

The period P_p for a 360° rotation in space of the lunar perigee, termed the lunar apsides cycle, is given by

$$P_p = \frac{Y_t}{Y_t - Y_s}, \qquad (2)$$

where Y_t and Y_s are the number of synodic months in the tidal year and solar year, respectively. As $Y_t = 14.6 \pm 0.1$ synodic months and $Y_s = 13.1 \pm 0.1$ synodic months at ~620 Ma, the period of the paleolunar apsides cycle was 9.7 ± 0.1 years.

The period of the lunar nodal cycle (the period of precession of the lunar orbital plane relative to the ecliptic plane, or revolution of the Moon's nodes), which is the most important long-term tidal constituent, evidently is recorded by the Elatina rhythmites. Because the lunar orbital plane is inclined at 5.15° to the ecliptic plane, the lunar declination (the angle between the lunar
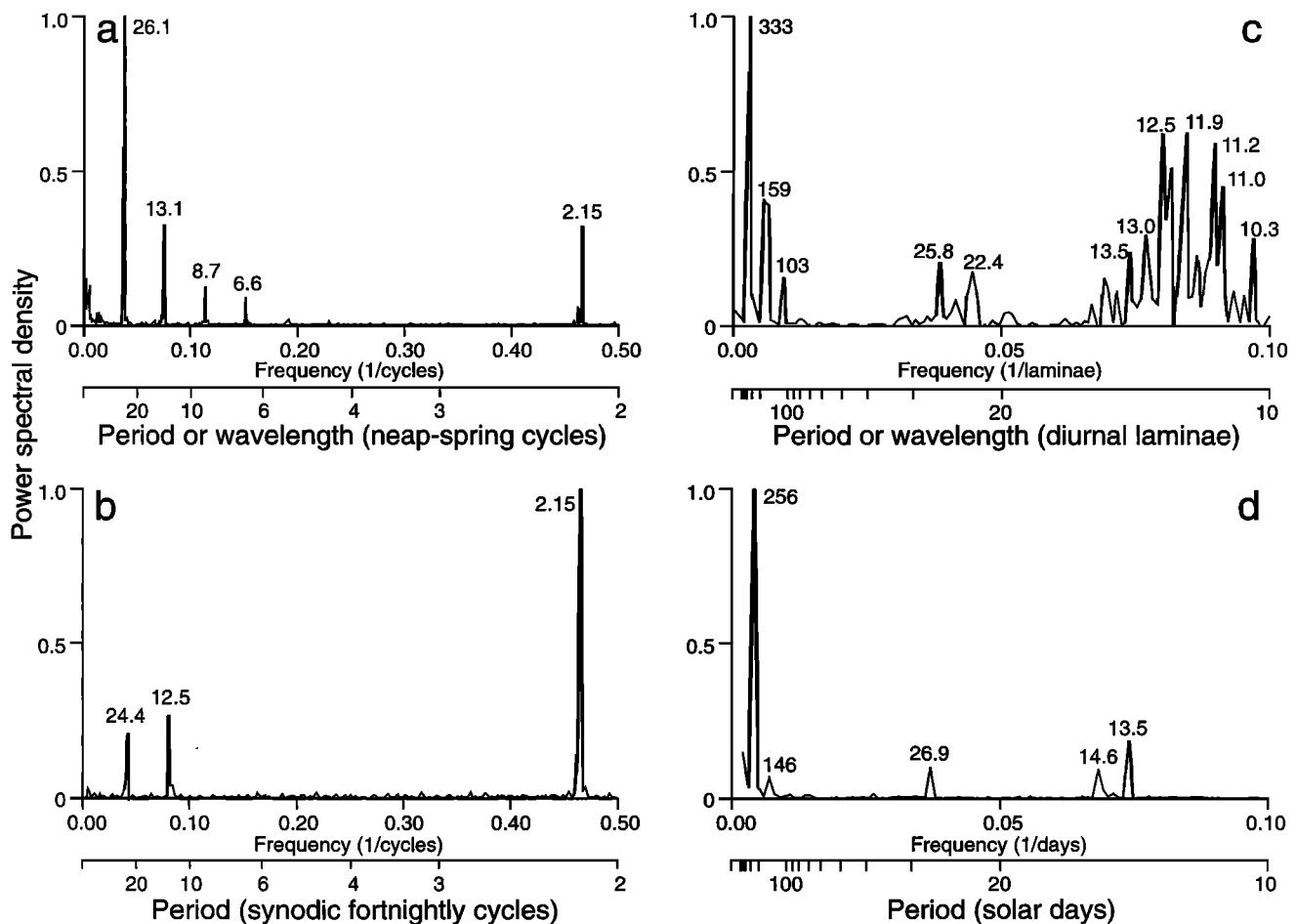
Figure 10. Fourier transform spectra for tidal and paleotidal sequential data, with power spectral densities normalized to unity for the strongest peak in each spectrum. (a) Elatina 60-year record of 1580 neap-spring cycle thickness measurements. The peaks at 26.1 and 13.1 neap-spring cycles represent annual and semiannual periods, and harmonics at 8.7 and 6.6 cycles the beating among the annual and semiannual signals and their combination tones. The peak near two neap-spring cycles records the monthly inequality of alternately thick and thin neap-spring cycles. (b) Maximum height of 495 spring tides (average of the two highest readings for each spring tide) at Townsville for 20 years from January 1, 1966, to December 31, 1985. The peaks at 24.4 and 12.5 synodic fortnightly cycles represent annual and semiannual periods, and the peak near two fortnightly cycles represents the monthly inequality of spring tides resulting from the elliptical lunar orbit. (c) Elatina record of 1337 diurnal lamina thickness measurements (4.2-year record, abbreviated at positions of neap tides). Peaks at 333 and 159 diurnal laminae represent the annual oscillation of sea level and the semiannual tidal cycle, and peaks from 10.3 to 13.5 diurnal laminae represent the neap-spring cycle (compare with 14–15 diurnal laminae per neap-spring cycle obtained from direct counts of the coeval Reynella rhythmites). Peaks at 22.4–25.8 diurnal laminae represent the anomalistic month (perigee to perigee), also shifted to higher frequencies. (d) Maximum daily height of sea level (average of the two highest daily readings) at Weipa for 2.8 years from April 5, 1985. The peaks at 256 and 146 days represent the annual oscillation and the semiannual tidal cycle, the peak at 26.9 days represents the anomalistic month (true period of 27.55 days), the peak at 14.6 days represents the synodic fortnight (14.77 days), and the peak at 13.5 days represents the tropical fortnight of varying lunar declination (13.66 days).

orbital plane and Earth's equatorial plane, which, on average, is 23.44°) varies between 18.29° and 28.59° with a period that is now 18.61 years. The 60-year Elatina record of neap-spring cycle thickness reveals a long-term period of 19.5 ± 0.5 years by variation in the height of the semiannual peaks, as measured from the base of the preceding trough to the top of the peak (Figure 9). A period near 19.5 years is confirmed by spectral analysis

of the Elatina data. The 20-year tidal record for Townsville is too short to warrant analysis for evidence of the nodal cycle, so a different tidal record was sought for comparison. The 18.6-year lunar nodal cycle dominates the annual means of high water, low water, and tidal range at Boston and other east coast harbors of the United States [*Kaye and Stuckey*, 1973] and modulates tidal heights, current strengths, and tide-influenced dep-

TABLE 1. Paleotidal and Paleorotational Values for Precambrian Cyclic Rhythmites and Modern Values

Parameter/Age	2450 Ma*	2450 Ma†	~900 Ma‡	~900 Ma§	~620 Ma‖	Modern
Lunar days per synodic month	(31.7 ± 3.0)	(31.1 ± 1.5)	(31.4 ± 1.1)	(30.3)	29.5 ± 0.5¶	28.53
Solar days per synodic month	(32.7 ± 3.0)	(32.1 ± 1.5)	(32.4 ± 1.1)	(31.3)	30.5 ± 0.5	29.53
Solar days per sidereal month	(30.7 ± 3.5)	(30.0 ± 1.7)	(30.3 ± 1.0)	(29.1)	28.3 ± 0.5	27.32
Synodic months per year	(15.7 ± 1.1)	14.5 ± 0.5¶	(14.3 ± 0.6)	13.5¶	13.1 ± 0.1¶	12.37
Sidereal months per year	(16.7 ± 1.1)	(15.5 ± 0.5)	(15.3 ± 0.6)	14.5	14.1 ± 0.1	13.37
Lunar apsides period (years)					9.7 ± 0.1¶	8.85
Lunar nodal period (years)	23.3 ± 1.5¶	(21.6 ± 0.7)	(21.5 ± 0.3)	(20.2)	19.5 ± 0.5¶	18.61
Solar days per year	(514 ± 33)	(466 ± 15)	464 ± 13	(422)	400 ± 7	365.24
Sidereal days per year	(515 ± 33)	(467 ± 15)	(465 ± 13)	(423)	401 ± 7	366.24
Length of solar day (hours)	(17.1 ± 1.1)	(18.8 ± 0.6)	18.9 ± 0.5	(20.8)	21.9 ± 0.4	24.00
Lunar semimajor axis (R_E)	(51.9 ± 3.3)	(54.6 ± 1.8)	54.7 ± 0.7	(57.1)	58.16 ± 0.30	60.27
Lunar recession rate (cm/yr)	(2.18 ± 0.86)	(1.47 ± 0.46)	(3.95 ± 0.5)	(2.25)	2.17 ± 0.31	3.82 ± 0.07**

Tidal and rotational values vary with time, but the length of the year is taken as constant (see section 4). The values in parentheses in columns 2–5 were derived by the present author from each primary or given value by applying equations (1), (3), (4), and (5) where appropriate and make allowance for the solar tide's contribution to the loss of angular momentum of Earth's rotation. Lunar recession rates are from given age to present; modern rate is obtained by laser ranging.

*Cyclic banded iron formation of the Weeli Wolli Formation, Western Australia, with lamina couplets viewed as annual increments grouped in paleolunar nodal cycles [Walker and Zahnle, 1986]. Error is ±1σ for the primary value, determined by the present author from the data used by Trendall [1973].

†Cyclic banded iron formation of the Weeli Wolli Formation, with lamina couplets viewed as synodic fortnightly increments grouped in annual cycles [Williams, 1989c, 1990]. Error is estimated for the primary value.

‡Rhythmites of the Big Cottonwood Formation, Utah [Sonett and Chan, 1998]. The given synodic period is 25.49 ± 0.5 "present epoch days"; primary neap-spring period is not available. Small internal discrepancies occur in the values given by Sonett and Chan [1998]. Errors are ±1σ.

§Rhythmites of the Big Cottonwood Formation, Utah [Sonett et al., 1996b]. Error for the primary value is not available.

‖Rhythmites of the Elatina Formation and Reynella Siltstone, South Australia [Williams, 1989a, b, c, 1990, 1991, 1994, 1997]. The rhythmites also record semidiurnal and diurnal increments and fortnightly, semiannual, and annual periods. Errors are ±1σ for primary values, except those for lunar days per synodic month and the lunar nodal period, which are estimates.

¶Primary value determined directly from the rhythmite record.

**From Dickey et al. [1994].

osition along the coast of the Dutch barrier islands [Oost et al., 1993]. The curve of variation in height of the semiannual peak in the Elatina record (Figure 13a) is comparable to that of annual mean tidal range for Boston for 1922–1970 (Figure 13b). Hence the long-term period of 19.5 ± 0.5 years identified in the Elatina record is interpreted as that of the paleolunar nodal cycle [Williams, 1989a, b, c].

Rhythmites interpreted as tidal in origin occur in early Neoproterozoic (900 ± 100 Ma) siltstone and silicified sandstone of the Big Cottonwood Formation in Big Cottonwood Canyon, central Utah [Chan et al., 1994]. These rhythmites have provided conflicting paleorotational values evidently because the raw data are abbreviated. Paleotidal and paleorotational values, including 18.2 h/d and 481 solar days/yr, initially were derived from lamina counts of Big Cottonwood neap-spring cycles [Sonett et al., 1996a]. However, a photograph of the rhythmites studied by Sonett et al. [1996a] shows that the neap-spring cycles contain as few as 4–5 sandstone laminae and are bounded by thick mud drapes at positions of neap tides, implying that the rhythmites are strongly abbreviated. Sonett et al. [1996b] later agreed that the Big Cottonwood rhythmites they studied initially are indeed strongly abbreviated at positions of neap tides, withdrawing the earlier results and providing a "corrected" value of 13.5 synodic months/yr for other Big Cottonwood rhythmites that they regarded as unabbreviated. That corrected primary value implies 20.8 h/d

and 422 solar days/yr at ~900 Ma (Table 1, column 5). Subsequently, Sonett and Chan [1998] examined further neap-spring cycles from the Big Cottonwood rhythmites that they also regarded as unabbreviated and derived values of 18.9 h/d and 464 solar days/yr (Table 1, column 4). These values are close to those initially proposed for the Big Cottonwood rhythmites and later withdrawn because the rhythmites are abbreviated. The two data sets given in Table 1 for the Big Cottonwood rhythmites disagree, and the dynamical implications of the latest results (column 4) are noted in section 5.2.

3.2. Validity of Neoproterozoic Values

Because tidal rhythmites may be abbreviated and so yield corrupted data, the validity of determined paleotidal and paleorotational values should be investigated where possible by testing for internal self-consistency through application of the laws of celestial mechanics. In demonstrating this procedure, three independent values that have been determined directly from the Elatina-Reynella rhythmite record are used to calculate the lunar semimajor axis (mean Earth-Moon distance) at ~620 Ma [Deubner, 1990; Williams, 1990, 1997].

The period of precession of the Moon's orbit depends on the Earth-Moon distance and can be expressed as

$$P = P_0(\cos i_0/\cos i)(a_0/a)^{1.5}, \qquad (3)$$

where P_0 is the present lunar nodal period of 18.61 years, P is the past lunar nodal period, a_0 is the present

semimajor axis of 60.27 R_E (units of Earth radius), a is the past lunar semimajor axis, i_0 is the present inclination of the lunar orbital plane to the ecliptic plane, and i is the past lunar inclination [*Walker and Zahnle*, 1986]. Assuming that the lunar inclination i has undergone negligible evolutionary change over the time interval in question [*Goldreich*, 1966], the paleolunar nodal period of 19.5 ± 0.5 years as indicated by the Elatina rhythmites gives $a/a_0 = 0.969 \pm 0.017$ at ~620 Ma [*Williams*, 1989a].

Kepler's third law states that the square of the orbital period of a planet is proportional to the cube of its mean distance from the Sun. In terms of the Earth-Moon system this law can be expressed as

$$(T_s/T_0)^2 = (a/a_0)^3, \tag{4}$$

where T_s is the length of the sidereal month in the past and T_0 is the present length of the sidereal month. From Table 1 (column 6), $T_s/T_0 = 13.37/(14.1 \pm 0.1)$, which gives $a/a_0 = 0.965 \pm 0.005$ at ~620 Ma.
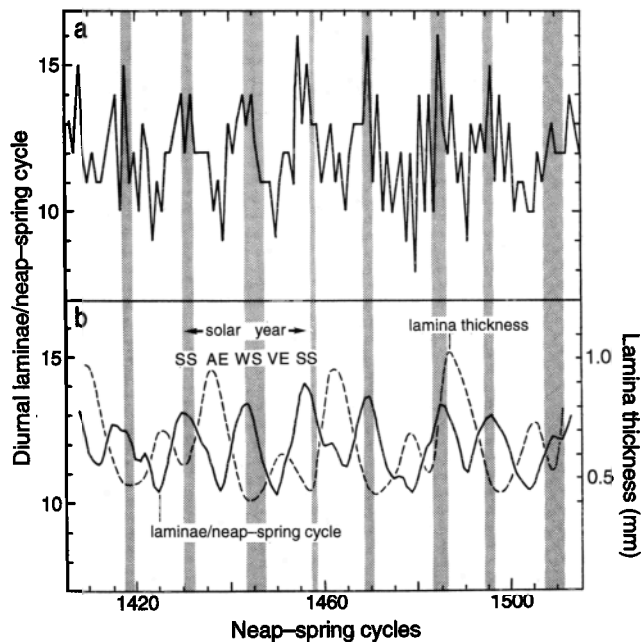

Figure 11. The number of diurnal laminae per neap-spring cycle counted between lamina thickness minima, for 110 neap-spring cycles (neap-spring cycle numbers are for the Elatina 60-year record and increase up the stratigraphic succession). (a) Unsmoothed curve. (b) Smoothed curves. The continuous curve (five-point filter weighted 1, 4, 6, 4, 1) shows that the number of diurnal laminae deposited per neap-spring cycle was strongly modulated by the semiannual tidal cycle (period ~13 neap-spring cycles). The dashed curve shows diurnal lamina thickness for the same stratigraphic interval (smoothed by 111-point filter). The shaded bands mark the stratigraphic positions of neap-spring cycles bounded by very thin silty laminae rather than mud drapes (Figure 4c). SS, summer solstice; WS, winter solstice; AE, autumnal equinox; VE, vernal equinox. See section 3.1 for full explanation. Modified from *Williams* [1991] and reproduced with the permission of the Canadian Society of Petroleum Geologists, Calgary.
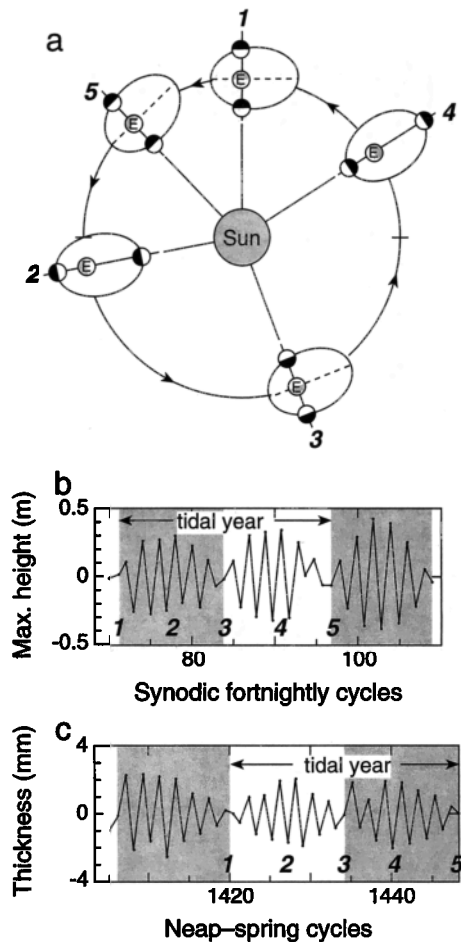

Figure 12. The Moon's orbit and synodic fortnightly tidal patterns for one "tidal year." (a) Schematic conjunctions and oppositions of the Moon and the Sun: positions 2 and 4, maximum monthly inequality of spring tidal height for successive conjunctions and oppositions, plotting as a sawtooth pattern in Figure 12b; positions 1, 3, and 5, minimum monthly inequality of spring tidal height and 180° change in phase of the sawtooth pattern. The tidal year (positions 1-5) is longer than the solar year because of prograde rotation in space of the lunar perigee. (b) Relative height of spring tides at Townsville over 1 tidal year (see Figure 8c); numbers 1-5 refer to positions of the Moon's orbit during one tidal year shown in Figure 12a. (c) Relative thickness of fortnightly neap-spring cycles in the Elatina rhythmites during 1 tidal year (see Figure 7c); numbers 1-5 refer to positions of the Moon's orbit during 1 tidal year shown in Figure 12a. The boundaries between shaded and unshaded areas in Figures 12b and 12c mark positions of 180° phase reversals in the sawtooth patterns. Modified from *Williams* [1991] and reproduced with the permission of the Canadian Society of Petroleum Geologists, Calgary.

The loss of Earth's rotational angular momentum through tidal friction of the Moon and the Sun and the change in lunar orbital angular momentum can be expressed as

$$1.219 - \frac{1}{4.93}\frac{\omega}{\omega_0} = \left(\frac{a}{a_0}\right)^{1/2} + \frac{(0.46)^2}{13}\left(\frac{a}{a_0}\right)^{13/2}, \tag{5}$$
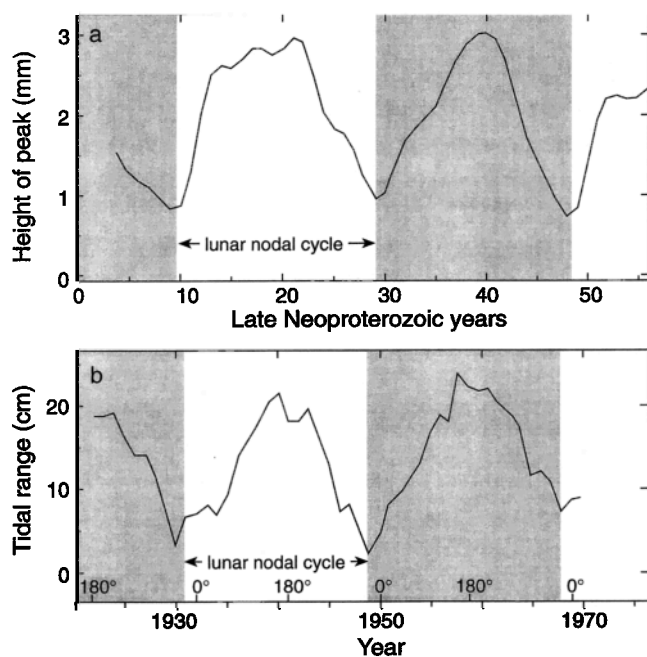
Figure 13. (a) Smoothed curve (seven-point weighted filter) of the height of the second-order peaks of neap-spring cycle thickness in the Elatina rhythmite record (see section 3.1 and Figure 9 for explanation). The height is modulated by a period of 19.5 ± 0.5 years. (b) Annual mean tidal range for Boston for 1922–1970, which is dominated by the 18.6-year lunar nodal cycle [from *Kaye and Stuckey*, 1973]. Times when the Moon's nodes were 0° and 180° in longitude are indicated. Modified from *Williams* [1989c] and reproduced with the permission of the International Union of Geological Sciences.

where ω_0 and ω are Earth's present and past rotation rates and the present ratio of the Moon's orbital angular momentum to Earth's spin angular momentum is 4.93 [*Deubner*, 1990]. From Table 1 (column 6), $\omega/\omega_0 = (401 \pm 7)/366.24$, which gives $a/a_0 = 0.968 \pm 0.007$ at ~620 Ma.

The above three determinations of the lunar semimajor axis are in close agreement (Table 2). This accordance of results, derived from independent, widely separated values by applying three different equations of celestial mechanics that make allowance for lunar and solar tidal effects, demonstrates the internal self-consistency of the observed Elatina-Reynella values and supports the validity of the paleotidal and paleorotational data set for ~620 Ma.

The validity of values determined for the Big Cottonwood rhythmites (Table 1, columns 4 and 5) cannot be investigated in this way because in each case only one primary value was determined directly from the rhythmites, with other values being derived from the primary value. Hence all the paleotidal and paleorotational values for ~900 Ma given in Table 1 are unverified. In view of the evidence for strong abbreviation of the Big Cottonwood rhythmites and the conflicting results, any paleotidal and paleorotational values obtained from those rhythmites should be viewed with caution until internal self-consistency of two or more different primary values is demonstrated.

The value of 400 ± 7 solar days/yr at ~620 Ma indicated by the Elatina-Reynella rhythmites conflicts with paleontological data for the early to middle Paleozoic, which suggest ~400–420 d/yr between 350 and 520 Ma (Figure 2). These particular values derived from fossils are of dubious reliability; two values have large errors, two other values are approximations, and five of the highest values are for maximum rather than mean counts. *Scrutton and Hipkin* [1973] and *Scrutton* [1978] argued that to accept only maximum counts for fossil data could lead to serious overestimates of the length of cycles if semidiurnal growth increments are counted inadvertently as diurnal increments. The value of ~435 (range 410–485) solar days/yr based on counts of presumed daily laminae in a columnar stromatolite claimed to be from the ~850-Ma Bitter Springs Formation in the Amadeus Basin, central Australia [*Vanyo and Awramik*, 1985], also must be queried. Subsequent detailed fieldwork has indicated that the stromatolite studied by *Vanyo and Awramik* [1985] is from the late Neoproterozoic Olympic Formation (M. R. Walter and R. J. F. Jenkins, personal communications, 1998), which is broadly coeval with or slightly younger than the ~620-Ma Reynella Siltstone and Elatina Formation in South Australia. The value of ~435 d/yr given by *Vanyo and Awramik* [1985], when plotted at this revised age (Figure 2, inset), conflicts with the Elatina-Reynella datum of 400 ± 7 solar days/yr.

Because internal self-consistency is demonstrable only for the Elatina-Reynella data set and because of the many doubts expressed concerning the reliability of stro-

TABLE 2. Lunar Semimajor Axis (Mean Earth-Moon Distance) at ~620 Ma and Mean Rate of Lunar Recession for the Past 620 Myr Indicated by the Elatina and Reynella Tidal Rhythmites

Paleotidal and Paleorotational Values	Lunar Semimajor Axis		Mean Rate of Lunar Recession, cm/yr*
	a/a_0	R_E	
19.5 ± 0.5 years (lunar nodal period)	0.969 ± 0.017	58.40 ± 1.02	1.92 ± 1.05
14.1 ± 0.1 sidereal months/yr	0.965 ± 0.005†	58.16 ± 0.30†	2.17 ± 0.31†
401 ± 7 sidereal days/yr	0.968 ± 0.007‡	58.34 ± 0.42‡	1.98 ± 0.43‡

Paleotidal and paleorotational values are from Table 1, column 6. Ratio a/a_0 is the ratio of the past to the present lunar semimajor axis.
*Lunar semimajor axis of 384,400 km [*Yoder*, 1995].
†Preferred value, based on best constrained primary data obtained by spectral analysis of the Elatina 60-year record.
‡Allows for the solar tide's contribution to the loss of angular momentum of Earth's rotation.
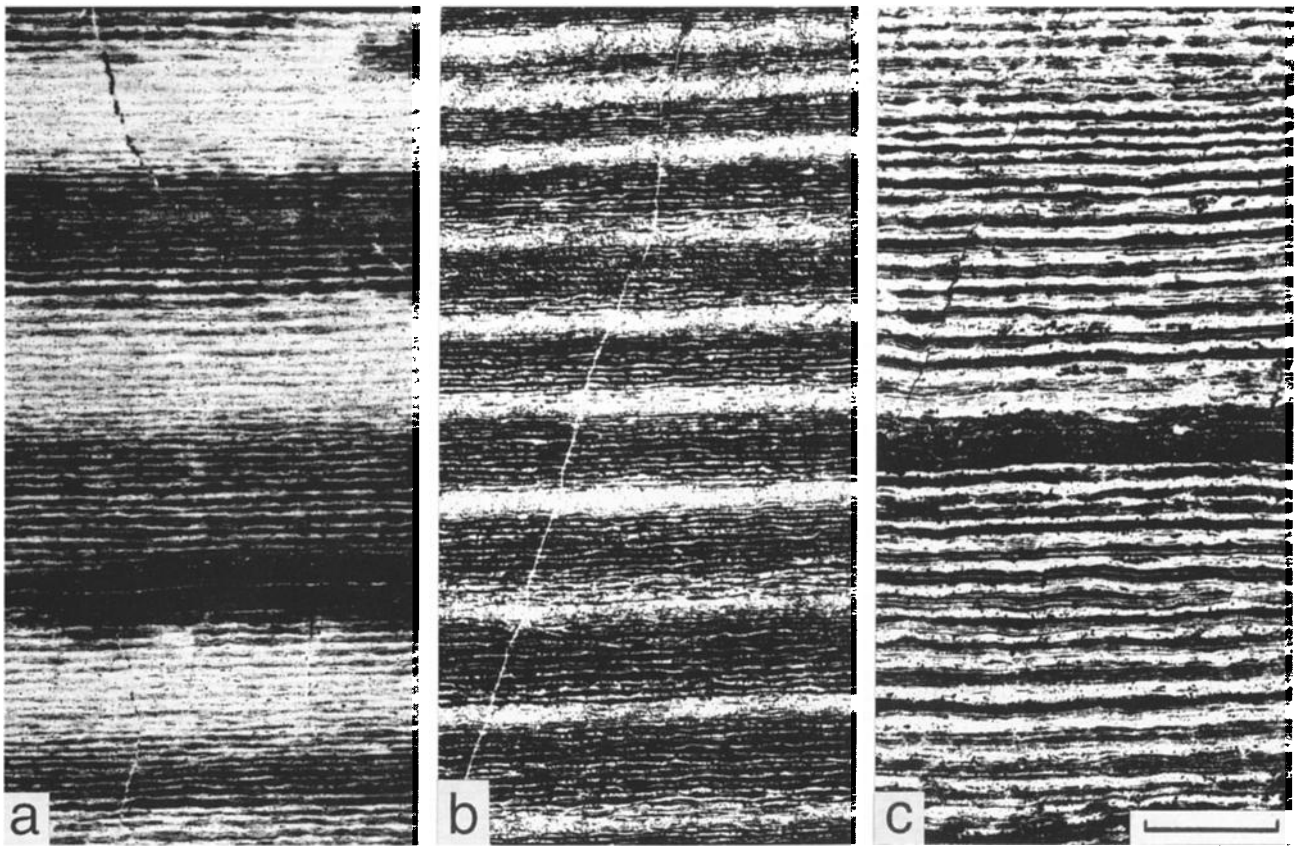
Figure 14. Paleoproterozoic (2450 Ma) cyclic banded iron formation from the Weeli Wolli Formation, Hamersley Basin, Western Australia. Scale bar is 5 mm. (a) Little compacted chert nodule containing discernible lamina couplets of chert (white) and iron oxide (black); up to 28–30 couplets occur between the centers of the cyclic "stripes." (b) Moderately compacted iron formation with thinner laminae and cyclic stripes. (c) Compacted iron formation in which only the cyclic stripes are readily discernible. Modified from *Williams* [1989c] and reproduced with the permission of the International Union of Geological Sciences.

matolite paleorotational data and paleontological clocks in general (see section 1), the value of 400 ± 7 solar days/yr and a l.o.d. of 21.9 ± 0.4 hours at ~620 Ma should be viewed as the only validated paleorotational data currently available for the Neoproterozoic and early to middle Paleozoic (1000–350 Ma).

3.3. Paleoproterozoic Tidal and Rotational Values

Paleotidal and paleorotational data are unavailable for the Mesoproterozoic (1600–1000 Ma) and are sparse for the Paleoproterozoic (2500–1600 Ma). The patterns of growth layers in Paleoproterozoic (~2000 Ma) stromatolites have yielded conflicting interpretations [*Pannella*, 1972a, b; *Mohr*, 1975], and *Lambeck* [1980] concluded that little confidence can be placed in the results. I have identified sandstone-mudstone cyclic rhythmites evidently of tidal origin in Paleoproterozoic (~2350 Ma) strata in Ontario, Canada, but these deposits contain erosional breaks and abbreviations and have yet to provide usable paleotidal values. A more promising source of paleotidal information is the conspicuous cyclicity displayed by Paleoproterozoic banded iron formation of the Weeli Wolli Formation in the Hamersley

Basin, Western Australia. This chemical deposit of very finely crystalline silica (chert) and iron oxides is dated at 2450 Ma [*Barley et al.*, 1997] and is thought to have been derived directly from submarine hydrothermal plumes generated at mid-ocean ridge crests or from heated marine waters of volcanic origin [e.g., *Isley*, 1995; *Barley et al.*, 1997]. Importantly, hydrothermal activity at a modern mid-ocean ridge crest shows tide-related variability, which suggests that the Weeli Wolli cyclicity may be of tidal origin and record paleotidal rhythms.

The Paleoproterozoic banded iron formations in Western Australia display lamina couplets, usually termed "microbands," that typically comprise a pale lamina of chert and a dark or opaque lamina of iron oxide [*Trendall and Blockley*, 1970; *Trendall*, 1983], although more complex laminated internal structure is not uncommon. Microbands have a mean thickness of ~0.7–1.0 mm, with some as much as 1.7 mm thick, and generally are regarded as annual increments or "varves." The lamina couplets of the Weeli Wolli Formation differ from the usual microbands of other banded iron formations in commonly being much thinner and locally displaying a conspicuous cyclicity (Figure 14). The cyclicity

is caused by regular variations in thickness both of the chert and iron oxide laminae, giving the rocks a characteristic striped appearance. Usually, the lamina couplets are very thin (≤ 0.05 mm), and only the cyclic stripes are readily discernible (Figures 14b and 14c). Cherty nodules or concretions that formed soon after deposition have largely avoided compaction during burial metamorphism, however, and comprise lamina couplets up to 0.3–0.4 mm in thickness (Figure 14a) that are more easily counted. *Trendall* [1973] found 21–28 lamina couplets per cycle with an average of 23.3 ± 1.5 (error is ±1σ, determined by me from the data used by *Trendall* [1973]). Interpreting each couplet as a normal microband representing 1 year's accretion, *Trendall* [1973] suggested that the cyclicity records the double sunspot or Hale cycle, although he could find no evidence for the single sunspot cycle. *Walker and Zahnle* [1986] also accepted an annual origin for the lamina couplets and the mean period of 23.3 years as determined by *Trendall* [1973] but interpreted the cyclicity as reflecting a climatic influence of the lunar nodal cycle.

Further counts of laminae I have carried out on enlarged photographs of thin sections of little compacted nodules containing up to 6–8 cycles indicate as many as 28–30 lamina couplets per cycle in the Weeli Wolli Formation [*Williams*, 1989c, 1990]. Cycles containing fewer lamina couplets may be abbreviated through nondeposition or by the amalgamation of laminae during burial metamorphism, and so counts for some cycles may underestimate the true cycle period. Hence a cycle period of 28–30 lamina couplets should be considered, and other explanations should be sought for the cyclicity.

Deep-sea monitoring over intervals of several weeks has revealed tidal influences on the discharge and dispersal of submarine hydrothermal plumes. At the trans-Atlantic geotraverse (TAG) hydrothermal mound on the Mid-Atlantic Ridge near 26°N, pressure pulses correspond to cycles of hydrothermal upflow with semidiurnal periodicity that are correlated with areal crustal strain caused by variations in tidal loading and Earth tides [*Nishizawa et al.*, 1995; *Fujioka et al.*, 1997]. Furthermore, nonbuoyant effluent at the TAG hydrothermal mound is periodically advected by prevailing semidiurnal and diurnal tidal currents near the seafloor [*Kinoshita et al.*, 1998]. The monitoring intervals were too brief to permit the reliable identification of any longer tidal periods. These observations at one of the world's largest submarine hydrothermal vent systems give credence to a tidal interpretation of the Weeli Wolli cyclicity, whereby tidal rhythms modulated the submarine discharge and/or dispersal of hydrothermal plumes during the Paleoproterozoic.

The following tidal interpretations of the Weeli Wolli lamina couplets therefore are suggested: (1) The lamina couplets are diurnal increments arranged in monthly cycles [*Cisne*, 1984]. Alternatively, the lamina couplets are semidiurnal increments grouped in fortnightly cycles. By these interpretations there were ~28–30 lunar

days per synodic month at 2450 Ma. (2) The lamina couplets are fortnightly increments arranged in annual cycles, the latter reflecting a seasonal influence on deposition. An annual period for the cyclicity implies that there were ~28–30 fortnightly cycles, or 14.5 ± 0.5 synodic months, per year at 2450 Ma. This interpretation of the Weeli Wolli cyclicity is consistent with the common occurrence in associated iron formations of complex microbands, viewed as annual increments, containing as many as 27 laminae that "may indicate short-term variations within seasons" [*Ewers and Morris*, 1981, p. 1947].

The several tidal and nontidal interpretations of the Weeli Wolli cyclicity employ timescales that differ by up to 3 orders of magnitude, and hence the plausibility of the implied rates of deposition should be considered when discriminating among the various ideas. Importantly, only the interpretation of 28–30 fortnightly increments arranged in annual cycles gives an effective rate of deposition for the compacted iron formation (Figure 14c) that is compatible with presumed rates of deposition for other compacted iron formations in the Hamersley Basin whose microbands are regarded as annual [*Trendall and Blockley*, 1970].

Additional paleotidal and paleorotational values for 2450 Ma that are derived from the preferred estimate of 14.5 ± 0.5 synodic months/yr by applying equations (1), (3), (4), and (5) are given in Table 1 (column 3). Values derived from a postulated period of 23.3 years for the lunar nodal cycle at 2450 Ma [*Walker and Zahnle*, 1986] are included for comparison (Table 1, column 2). All these suggested values for 2450 Ma are unverified. A self-consistent set of paleotidal and paleorotational values measured directly from a Paleoproterozoic rhythmite record is required to establish with reasonable confidence the number of days per year, l.o.d., and the Moon's orbit for that early time.

4. EARTH'S MOMENT OF INERTIA AND PALEORADIUS

Runcorn [1964, 1966] showed how paleotidal and paleorotational data can be used to explore whether Earth's moment of inertia has changed over geological time. Such analysis also can examine whether Earth's radius has increased significantly with time, as required by the hypothesis of Earth expansion, because Earth's moment of inertia would increase with secular increase in radius. From *Runcorn* [1964, 1966],

$$1 - \frac{L}{L_0} = \left(-1 + \frac{I}{I_0} \frac{\omega}{\omega_0} \frac{Y_0}{Y} \right) \Big/ 4.93(1 + \beta), \quad (6)$$

where L/L_0 is the ratio of the past to the present lunar orbital angular momentum, I_0 and I are Earth's present and past moments of inertia, ω_0 and ω are Earth's present and past rotation rates, Y_0 and Y are the lengths

of the present and past year, β is the present ratio of solar to lunar retarding torques acting on Earth, 4.93 is the present ratio of the Moon's orbital angular momentum to Earth's spin angular momentum, and

$$\left(\frac{L_0}{L}\right)^3 = \frac{T_0}{Y_0}\frac{\omega}{t_s},$$

T_0 being the present length of the sidereal month and t_s being the number of solar days per sidereal month in the past.

The Elatina-Reynella data set (Table 1, column 6) can reveal whether Earth's moment of inertia has changed significantly since ~620 Ma. If $Y = Y_0$, implying no secular change in the universal gravitational parameter G, the appropriate Elatina-Reynella values provide the following figures for I/I_0 using different estimates of β: (1) $I/I_0 = 1.012 \pm 0.018$ (for $\beta = 1/5.1$ [Munk and MacDonald, 1960]). (2) $I/I_0 = 1.011 \pm 0.018$ and 1.018 ± 0.018 (for $\beta = 1/5.5$ and $1/3.7$, respectively [Runcorn, 1966]). (3) $I/I_0 = 1.014 \pm 0.018$ (for $\beta = 1/4.6$ [Lambeck, 1980]). (4) $I/I_0 = 1.006 \pm 0.018$ (for $\beta = 1/8.2$ [Brosche and Wünsch, 1990]).

These figures are the only available direct estimates of I/I_0 for the Precambrian and argue against significant overall change in Earth's moment of inertia since ~620 Ma. Moreover, they rule out rapid Earth expansion since that time by endogenous (noncosmological) mechanisms, particularly the hypothesis of rapid expansion since the Paleozoic [Carey, 1958, 1976], which requires $I/I_0 = 0.5$ [Runcorn, 1964]. The figures for I/I_0 determined here also argue against slow expansion by endogenous mechanisms. A proposed increase in radius of 0.50–0.95 mm/yr [Creer, 1965] gives $I/I_0 = 0.89$–0.94, and the postulate that Earth's radius has increased by 0.65 ± 0.15 mm/yr for at least the past 600 Myr [Egyed, 1969] gives $I/I_0 = 0.91$–0.94. The suggestion of Carey [1976] that substantial Earth expansion may have resulted from change of phase of minerals in Earth's interior to their less dense forms caused by a postulated secular decrease in G, i.e., $Y \ll Y_0$, is not supported by studies of the morphologies of Mercury, Mars, and the Moon; those bodies also would have been affected by decrease in G but show little or no evidence of expansion [Crossley and Stevens, 1976; McElhinny et al., 1978]. Moreover, Mars Viking Lander and lunar laser-ranging data indicate negligible change in planetary orbital radii, which implies negligible change in the length of the year and in G [Hellings et al., 1983; Chandler et al., 1993; Dickey et al., 1994]. Hence the rhythmite data and the astronomical and astrometric observations together argue against significant change in Earth's radius by any mechanism at least since ~620 Ma.

5. HISTORY OF THE MOON'S ORBIT

Paleotidal data recorded by cyclic tidal rhythmites promise to allow the evolving lunar orbit, including the

mean Earth-Moon distance near the time of the Moon's origin around 4.5 Ga or an epoch of a possible close approach of the Moon, to be determined with reasonable accuracy.

5.1. Rates of Lunar Recession

Mean rates of lunar recession since Paleoproterozoic time as indicated by rhythmite data are given in Table 1. The mean Earth-Moon distance of 58.16 ± 0.30 R_E ($a/a_0 = 0.965 \pm 0.005$) at ~620 Ma, indicated by the Elatina value of 14.1 ± 0.1 sidereal months/yr (the best constrained parameter in Table 2), gives a mean rate of lunar recession of 2.17 ± 0.31 cm/yr over the past 620 Myr. This mean rate is ~57% of the present rate of lunar recession, or increase in the semimajor axis, of 3.82 ± 0.07 cm/yr obtained by lunar laser ranging [Dickey et al., 1994] and ~68% of the mean recession rate of ~3.16 cm/yr for the Phanerozoic suggested by paleontological data [Lambeck, 1980]. The preferred Weeli Wolli datum, for which the lamina couplets are viewed as fortnightly increments grouped in annual cycles (Table 1, column 3), gives, by Kepler's third law (4), a mean Earth-Moon distance of $54.6 \pm 1.8\,R_E$ ($a/a_0 = 0.906 \pm 0.029$) at 2450 Ma, suggesting an even lower mean rate of lunar recession of 1.47 ± 0.46 cm/yr over the past 2450 Myr. The Big Cottonwood data yield conflicting mean rates of lunar recession since ~900 Ma (Table 1, columns 4 and 5), with the mean rate of 3.95 ± 0.5 cm/yr (column 4) being at odds with other data for the Precambrian and carrying dubious dynamical implications (see section 5.2).

The combined Weeli Wolli and Elatina-Reynella data suggest a mean rate of lunar recession of 1.24 ± 0.71 cm/yr for most of the Proterozoic eon (2450–620 Ma). This figure is ~58% of the mean recession rate since 620 Ma and is only ~33% of the present recession rate. The suggested increasing mean rate of lunar recession since 2450 Ma is consistent with increasing oceanic tidal dissipation as Earth's rotation slows [see Hansen, 1982; Webb, 1982]. The present high rate of lunar recession may reflect the near resonance of oceanic free modes and tidal frequencies [Lambeck, 1980; Sündermann, 1982; Brosche, 1984].

5.2. Evolution of the Lunar Distance

Expressions that allow mean Earth-Moon distance in the past to be estimated from rate of lunar recession are provided by Walker and Zahnle [1986]. Considering only the lunar semidiurnal tide and neglecting the inclination and eccentricity of the Moon's orbit, the mean Earth-Moon distance a_T at an earlier time T is approximated by

$$a_T = a_0\left[1 - \frac{13}{2}\frac{\langle \dot{a}_0\rangle}{a_0}T\right]^{2/13}, \qquad (7)$$

where a_0 is the present mean Earth-Moon distance and $\langle\dot{a}_0\rangle$ is the mean rate of lunar recession. Projecting into
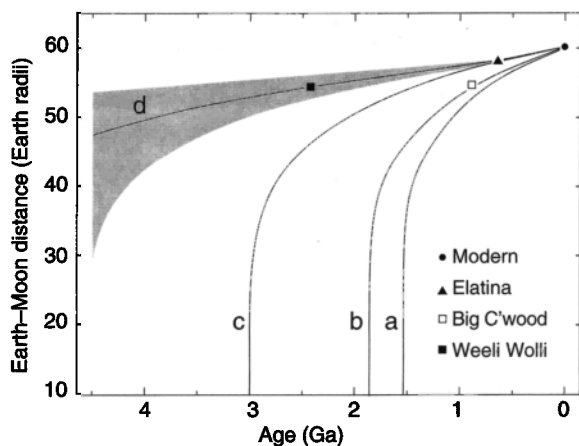
Figure 15. Change in mean Earth-Moon distance with time, as suggested by different average rates of tidal energy dissipation. Curve a employs a dissipation rate consistent with the present rate of lunar recession of 3.82 cm/yr [*Dickey et al.*, 1994] in equation (7). Curve b employs a dissipation rate consistent with a mean rate of lunar recession of 3.16 cm/yr since ~500 Ma suggested by paleontological data [*Lambeck*, 1980] in equation (7). The Big Cottonwood datum is from *Sonett and Chan* [1998] (Table 1, column 4). Curve c employs a dissipation rate consistent with the Elatina datum (Table 2) in equation (7). Curve d employs a dissipation rate consistent with the Elatina datum and the preferred Weeli Wolli datum (Table 1, column 3), in equation (8); shaded area shows the error based on the Weeli Wolli datum.

$$a_T = a_1 \left[1 - \frac{13}{2}(T - T_1)\frac{\langle \dot{a}_1 \rangle}{a_1} \right]^{2/13}, \qquad (8)$$

where a_1 is the mean Earth-Moon distance at time T_1 (620 Ma) and $\langle \dot{a}_1 \rangle$ represents a dissipation rate consistent with the Weeli Wolli and Elatina data equal to a lunar recession velocity of 3.3×10^{-8} cm/s. This tidal scenario suggests that a close approach of the Moon has not occurred at any time during Earth history (Figure 15, curve d). The findings, while tentative, are consistent with other tidal histories [e.g., *Hansen*, 1982; *Webb*, 1982].

The uncertainties in the available Paleoproterozoic paleotidal values are too great to permit a reasonable estimate of the mean Earth-Moon distance at 4.5 Ga. A demonstrably self-consistent paleotidal and paleorotational data set is required for the Archean or early Paleoproterozoic to allow the early history of the Moon's orbit to be traced with confidence.

6. CONCLUSIONS

Sedimentology offers a methodology for directly tracing the early history of Earth's tidal deceleration and the evolving lunar orbit through analysis of sedimentary tidal rhythmites. Cyclically laminated marginal marine deposits usually of sandstone, siltstone, and mudstone, whose rates of deposition were modulated by tidal cycles, have provided a rich paleotidal and paleorotational data set for the late Neoproterozoic (~620 Ma) that is demonstrably self-consistent through application of the laws of celestial mechanics. At that time there were 400 ± 7 solar days/yr and 13.1 ± 0.1 synodic months/yr, and the length of day was 21.9 ± 0.4 hours; the mean rate of lunar recession since that time is 2.17 ± 0.31 cm/yr, little more than half the present rate of lunar recession of 3.82 ± 0.07 cm/yr obtained by lunar laser ranging. The late Neoproterozoic rhythmite data do not support significant change in Earth's moment of inertia and radius over the past 620 Myr. Earlier paleotidal records are sparse and should be viewed with caution until internal self-consistency has been demonstrated. Conspicuously cyclic banded iron formation, however, may record paleotidal information for Paleoproterozoic time (2450 Ma). The available Proterozoic rhythmite data are consistent with an overall low rate of tidal friction and the long-term stability of the Moon's orbit.

Marginal marine deposits of tidal origin are common in the stratigraphic record, and geologists will likely discover many additional examples of cyclic tidal rhythmites. Special importance should be placed on the search for cyclic tidal rhythmites of Paleoproterozoic and Archean age that could provide internally self-consistent paleotidal and paleorotational values. The discovery and detailed study of such rhythmites would greatly extend our knowledge of the dynamical history of the Precambrian Earth-Moon system.

the past a rate of tidal energy dissipation consistent with the present rate of lunar recession of 3.82 cm/yr indicates a close approach of the Moon at ~1.5 Ga (Figure 15, curve a). Employing a tidal dissipation rate consistent with a mean rate of lunar recession of $~1.0 \times 10^{-7}$ cm/s (3.16 cm/yr) for the Phanerozoic suggested by paleontological data [*Lambeck*, 1980] gives a·close approach at ~1.9 Ga (Figure 15, curve b), as does the Big Cottonwood datum of *Sonett and Chan* [1998] (Table 1, column 4). By comparison, employing an average rate of tidal energy dissipation consistent with the Elatina datum of $a/a_0 = 0.965$ and the indicated mean rate of lunar recession of 2.17 cm/yr since 620 Ma (Tables 1 and 2) pushes back a possible close approach of the Moon to 3 Ga (Figure 15, curve c). However, the geological records of Earth and the Moon provide no evidence of such a cataclysm in the Archean or Paleoproterozoic, and additional paleotidal data are required for an epoch prior to ~620 Ma to permit the early history of the Moon's orbit to be traced more accurately.

The paleotidal datum for 2450 Ma suggested by the Weeli Wolli rhythmites where viewed as fortnightly increments grouped in annual cycles (Table 1, column 3) is used here with the Elatina datum for 620 Ma to demonstrate how the Moon's orbit may be traced beyond 3 Ga. From *Walker and Zahnle* [1986] the mean lunar distance prior to 620 Ma is approximated by

NOTATION

a_0 present mean Earth-Moon distance (semimajor axis of the Moon's orbit) of 384,400 km, equal to 60.27 R_E (units of Earth radius) [*Yoder*, 1995].

a mean Earth-Moon distance in the past.

a_T mean Earth-Moon distance at time T.

a_1 mean Earth-Moon distance at time T_1.

β present ratio of solar to lunar retarding torques acting on Earth.

δ lag angle between Earth's tidal bulge and the Earth-Moon axis.

i_0 present inclination of the lunar orbital plane to the ecliptic plane of 5.15°.

i past inclination of the lunar orbital plane to the ecliptic plane.

I/I_0 ratio of Earth's past and present moments of inertia.

L/L_0 ratio of the past to the present lunar orbital angular momentum.

P_0 present lunar nodal period of 18.61 years.

P past lunar nodal period.

P_p period for a 360° rotation in space of the lunar perigee.

R_E Earth's equatorial radius, 6378.14 km [*Yoder*, 1995].

t number of solar days per sidereal month.

t_L number of solar days per synodic (lunar) month.

t_s number of solar days per sidereal month in the past.

T_0 present length of the sidereal month.

T_s length of the sidereal month in the past.

T time of mean Earth-Moon distance a_T.

T_1 time of mean Earth-Moon distance a_1.

ω_0 Earth's present rotation rate.

ω Earth's past rotation rate.

Y_0 length of the present year.

Y length of the year in the past.

Y_D number of solar days in the year.

Y_s number of synodic months in the solar year.

Y_t number of synodic months in tne tidal year.

REFERENCES

Allen, J. R. L., Mud drapes in sand-wave deposits: A physical model with application to the Folkestone Beds (Early Cretaceous, southeast England), *Philos. Trans. R. Soc. London, Ser. A, 306*, 291–345, 1982.

Allen, J. R. L., Salt-marsh growth and stratification: A numerical model with special reference to the Severn Estuary, southwest Britain, *Mar. Geol., 95*, 77–96, 1990.

Barley, M. E., A. L. Pickard, and P. J. Sylvester, Emplacement of a large igneous province as a possible cause of banded iron formation 2.45 billion years ago, *Nature, 385*, 55–58, 1997.

Berry, A., *A Short History of Astronomy, From Earliest Times Through the Nineteenth Century*, John Murray, London, 1898. (Also published by Dover, Mineola,.N. Y., 1961).

Berry, W. B., and R. M. Barker, Fossil bivalve shells indicate longer month and year in Cretaceous than present, *Nature, 217*, 938–939, 1968.

Boersma, J. R., and J. H. J. Terwindt, Neap-spring tide sequences of intertidal shoal deposits in a mesotidal estuary, *Sedimentology, 28*, 151–170, 1981.

Boothroyd, J. C., Tidal inlets and tidal deltas, in *Coastal Sedimentary Environments*, edited by R. A. Davis, pp. 445–532, Springer-Verlag, New York, 1985.

Brosche, P., Tidal friction in the Earth-Moon system, *Philos. Trans. R. Soc. London, Ser. A, 313*, 71–75, 1984.

Brosche, P., and J. Wünsch, The solar torque: A leak for the angular momentum of the Earth-Moon system, in *Earth's Rotation from Eons to Days*, edited by P. Brosche and J. Sündermann, pp. 141–145, Springer-Verlag, New York, 1990.

Carey, S. W., A tectonic approach to continental drift, in *Continental Drift: A Symposium*, edited by S. W. Carey, pp. 177–355, Univ. of Tasmania, Hobart, Australia, 1958.

Carey, S. W., *The Expanding Earth*, 488 pp., Elsevier Sci., New York, 1976.

Chan, M. A., E. P. Kvale, A. W. Archer, and C. P. Sonett, Oldest direct evidence of lunar-solar tidal forcing in sedimentary rhythmites, Proterozoic Big Cottonwood Formation, central Utah, *Geology, 22*, 791–794, 1994.

Chandler, J. F., R. D. Reasenberg, and I. I. Shapiro, New bound on $\dot{G}$, *Bull. Am. Astron. Soc., 25*, 1233, 1993.

Cisne, J. L., A basin model for massive banded iron-formations and its geophysical applications, *J. Geol., 92*, 471–488, 1984.

Creer, K. M., An expanding Earth?, *Nature, 205*, 539–544, 1965.

Crisp, D. J., Tidally deposited bands in shells of barnacles and molluscs, in *Origin, Evolution, and Modern Aspects of Biomineralization in Plants and Animals*, edited by R. E. Crick, pp. 103–124, Plenum, New York, 1989.

Crossley, D. J., and R. K. Stevens, Expansion of the Earth due to a secular decrease in G: Evidence from Mercury, *Can. J. Earth Sci., 13*, 1723–1725, 1976.

Dalrymple, R. W., Y. Makino, and B. A. Zaitlin, Temporal and spatial patterns of rhythmite deposition on mud flats in the macrotidal Cobequid Bay-Salmon River estuary, Bay of Fundy, Canada, *Mem. Can. Soc. Pet. Geol., 16*, 137–160, 1991.

de Boer, P. L., A. P. Oost, and M. J. Visser, The diurnal

inequality of the tide as a parameter for recognizing tidal influences, *J. Sediment. Petrol.*, *59*, 912–921, 1989.

Delaunay, M., Sur l'existence d'une cause nouvelle ayant une influence sensible sur la valeur de l'equation séculaire de la Lune, *C. R. Hebd. Seances Acad. Sci.*, *61*, 1023–1032, 1865.

Deubner, F.-L., Discussion on Late Precambrian tidal rhythmites in South Australia and the history of the Earth's rotation, *J. Geol. Soc. London*, *147*, 1083–1084, 1990.

Deynoux, M., P. Duringer, R. Khatib, and M. Villeneuve, Laterally and vertically accreted tidal deposits in the Upper Proterozoic Madina-Kouta Basin, southeastern Senegal, West Africa, *Sediment. Geol.*, *84*, 179–188, 1993.

Dickey, J. O., et al., Lunar laser ranging: A continuing legacy of the Apollo program, *Science*, *265*, 482–490, 1994.

Egyed, L., The slow expansion hypothesis, in *The Application of Modern Physics to the Earth and Planetary Interiors*, edited by S. K. Runcorn, pp. 65–75, Wiley-Interscience, New York, 1969.

Eriksson, K. A., Tidal deposits from the Archaean Moodies Group, Barberton Mountain Land, South Africa, *Sediment. Geol.*, *18*, 257–281, 1977.

Ewers, W. E., and R. C. Morris, Studies of the Dales Gorge Member of the Brockman Iron Formation, Western Australia, *Econ. Geol.*, *76*, 1929–1953, 1981.

FitzGerald, D. M., and D. Nummedal, Response characteristics of an ebb-dominated tidal inlet channel, *J. Sediment. Petrol.*, *53*, 833–845, 1983.

Fujioka, K., K. Kobayashi, K. Kato, M. Aoki, K. Mitsuzawa, M. Kinoshita, and A. Nishizawa, Tide-related variability of TAG hydrothermal activity observed by deep-sea monitoring system and OBSH, *Earth Planet. Sci. Lett.*, *153*, 239–250, 1997.

Goldreich, P., History of the lunar orbit, *Rev. Geophys.*, *4*, 411–439, 1966.

Hambrey, M. J., and W. B. Harland (Eds.), *Earth's Pre-Pleistocene Glacial Record*, 1004 pp., Cambridge Univ. Press, New York, 1981.

Hansen, K. S., Secular effects of oceanic tidal dissipation on the Moon's orbit and the Earth's rotation, *Rev. Geophys.*, *20*, 457–480, 1982.

Hastie, W. (Ed.), *Kant's Cosmogony, As in his Essay on the Retardation of the Rotation of the Earth and his Natural History and Theory of the Heavens*, translated from German by W. Hastie, 205 pp., Maclehose, Glasgow, Scotland, 1900. (Also published by Thoemmes Press, Bristol, England, 1993.)

Hellings, R. W., P. J. Adams, J. D. Anderson, M. S. Keesey, E. L. Lau, E. M. Standish, V. M. Canuto, and I. Goldman, Experimental test of the variability of *G* using Viking Lander ranging data, *Phys. Rev. Lett.*, *51*, 1609–1612, 1983.

Hofmann, H. J., Stromatolites: Characteristics and utility, *Earth Sci. Rev.*, *9*, 339–373, 1973.

Imperato, D. P., W. J. Sexton, and M. O. Hayes, Stratigraphy and sediment characteristics of a mesotidal ebb-tidal delta, North Edisto Inlet, South Carolina, *J. Sediment. Petrol.*, *58*, 950–958, 1988.

Isley, A. E., Hydrothermal plumes and the delivery of iron to banded iron formation, *J. Geol.*, *103*, 169–185, 1995.

Kaye, C. A., and G. W. Stuckey, Nodal tidal cycle of 18.6 yr, *Geology*, *1*, 141–144, 1973.

Kinoshita, M., R. P. Von Herzen, O. Matsubayashi, and K. Fujioka, Tidally-driven effluent detected by long-term temperature monitoring at the TAG hydrothermal mound, Mid-Atlantic Ridge, *Phys. Earth Planet. Inter.*, *108*, 143–154, 1998.

Komar, P. D., and D. B. Enfield, Short-term sea-level changes and coastal erosion, in *Sea-Level Fluctuation and Coastal Evolution*, edited by D. Nummedal, O. H. Pilkey, and J. D.

Howard, *Spec. Publ. SEPM Soc. Sediment. Geol.*, *41*, 17–27, 1987.

Kuecher, G. J., B. G. Woodland, and F. M. Broadhurst, Evidence of deposition from individual tides and of tidal cycles from the Francis Creek Shale (host rocks to the Mazon Creek Biota), Westphalian D (Pennsylvanian), northeastern Illinois, *Sediment. Geol.*, *68*, 211–221, 1990.

Kvale, E. P., J. Cutright, D. Bilodeau, A. Archer, H. R. Johnson, and B. Pickett, Analysis of modern tides and implications for ancient tidalites, *Cont. Shelf Res.*, *15*, 1921–1943, 1995.

Lambeck, K., *The Earth's Variable Rotation: Geophysical Causes and Consequences*, 449 pp., Cambridge Univ. Press, New York, 1980.

MacDonald, G. J. F., Tidal friction, *Rev. Geophys.*, *2*, 467–541, 1964.

Martino, R. L., and D. D. Sanderson, Fourier and autocorrelation analysis of estuarine tidal rhythmites, lower Breathitt Formation (Pennsylvanian), eastern Kentucky, USA, *J. Sediment. Petrol.*, *63*, 105–119, 1993.

Mazzullo, S. J., Length of the year during the Silurian and Devonian Periods, *Geol. Soc. Am. Bull.*, *82*, 1085–1086, 1971.

McElhinny, M. W., S. R. Taylor, and D. J. Stevenson, Limits to the expansion of the Earth, Moon, Mars and Mercury and to changes in the gravitational constant, *Nature*, *271*, 316–321, 1978.

McGugan, A., Possible use of algal stromatolite rhythms in geochronology, *Spec. Pap. Geol. Soc. Am.*, *115*, 145, 1968.

Mohr, R. E., Measured periodicities of the Biwabik (Precambrian) stromatolites and their geophysical significance, in *Growth Rhythms and the History of the Earth's Rotation*, edited by G. D. Rosenberg and S. K. Runcorn, pp. 43–56, Wiley-Interscience, New York, 1975.

Munk, W., Once again: Tidal friction, *Q. J. R. Astron. Soc.*, *9*, 352–375, 1968.

Munk, W. H., and G. J. F. MacDonald, *The Rotation of the Earth*, 323 pp., Cambridge Univ. Press, New York, 1960.

Nio, S.-D., and C.-S. Yang, Diagnostic attributes of clastic tidal deposits: A review, in *Clastic Tidal Sedimentology*, edited by D. G. Smith et al., *Mem. Can. Soc. Pet. Geol.*, *16*, 3–27, 1991.

Nishizawa, A., T. Sato, J. Kasahara, and K. Fujioka, Hydrothermal activity correlated with tides on the TAG mound, MAR, detected by ocean bottom hydrophone, *Eos Trans. AGU*, *76*(46), Fall Meet. Suppl., F574, 1995.

Oost, A. P., H. de Haas, F. IJnsen, J. M. van den Boogert, and P. L. de Boer, The 18.6 yr nodal cycle and its impact on tidal sedimentation, *Sediment. Geol.*, *87*, 1–11, 1993.

Özsoy, E., Ebb-tidal jets: A model of suspended sediment and mass transport at tidal inlets, *Estuarine Coastal Shelf Sci.*, *22*, 45–62, 1986.

Pannella, G., Paleontological evidence on the Earth's rotational history since early Precambrian, *Astrophys. Space Sci.*, *16*, 212–237, 1972a.

Pannella, G., Precambrian stromatolites as paleontological clocks, *Int. Geol. Congr. Rep. Sess.*, *24*th, sect. 1, 50–57, 1972b.

Pariwono, J. I., J. A. T. Bye, and G. W. Lennon, Long-period variations of sea-level in Australasia, *Geophys. J. R. Astron. Soc.*, *87*, 43–54, 1986.

Preiss, W. V. (Compiler), The Adelaide Geosyncline, *S. Aust. Dep. Mines Energy Bull.*, *53*, 438 pp., 1987.

Reading, H. G. (Ed.), *Sedimentary Environments and Facies*, 557 pp., Blackwell, Malden, Mass., 1978.

Reineck, H.-E., and I. B. Singh, *Depositional Sedimentary Environments*, 439 pp., Springer-Verlag, New York, 1973.

Roep, Th. B., Neap-spring cycles in a subrecent tidal channel fill (3665 BP) at Schoorldam, NW Netherlands, *Sediment. Geol.*, *71*, 213–230, 1991.

Rosenberg, G. D., and S. K. Runcorn (Eds.), *Growth Rhythms and the History of the Earth's Rotation*, 559 pp., John Wiley, New York, 1975.

Runcorn, S. K., Changes in the Earth's moment of inertia, *Nature, 204*, 823–825, 1964.

Runcorn, S. K., Change in the moment of inertia of the Earth as a result of a growing core, in *The Earth-Moon System*, edited by B. G. Marsden and A. G. W. Cameron, pp. 82–92, Plenum, New York, 1966.

Runcorn, S. K., Palaeontological data on the history of the Earth-Moon system, *Phys. Earth Planet. Inter., 20*, p1–p5, 1979.

Scrutton, C. T., Periodic growth features in fossil organisms and the length of the day and month, in *Tidal Friction and the Earth's Rotation*, edited by P. Brosche and J. Sünder-mann, pp. 154–196, Springer-Verlag, New York, 1978.

Scrutton, C. T., and R. G. Hipkin, Long-term changes in the rotation rate of the Earth, *Earth Sci. Rev., 9*, 259–274, 1973.

Smith, D. G., G. E. Reinson, B. A. Zaitlin, and R. A. Rahmani (Eds.), *Clastic Tidal Sedimentology, Mem. Can. Soc. Pet. Geol., 16*, 387 pp., 1991.

Smith, N. D., A. C. Phillips, and R. D. Powell, Tidal drawdown: A mechanism for producing cyclic sediment laminations in glaciomarine deltas, *Geology, 18*, 10–13, 1990.

Sonett, C. P., and M. A. Chan, Neoproterozoic Earth-Moon dynamics: Rework of the 900 Ma Big Cottonwood Canyon tidal rhythmites, *Geophys. Res. Lett., 25*, 539–542, 1998.

Sonett, C. P., E. P. Kvale, A. Zakharian, M. A. Chan, and T. M. Demko, Late Proterozoic and Palaeozoic tides, retreat of the Moon, and rotation of the Earth, *Science, 273*, 100–104, 1996a.

Sonett, C. P., A. Zakharian, and E. P. Kvale, Ancient tides and length of day: Correction, *Science, 274*, 1068–1069, 1996b.

Sündermann, J., The resonance behaviour of the world ocean, in *Tidal Friction and the Earth's Rotation II*, edited by P. Brosche and J. Sündermann, pp. 165–174, Springer-Verlag, New York, 1982.

Tessier, B., Upper intertidal rhythmites in the Mont-Saint-Michel Bay (NW France): Perspectives for paleorecon-struction, *Mar. Geol., 110*, 355–367, 1993.

Trendall, A. F., Varve cycles in the Weeli Wolli Formation of the Precambrian Hamersley Group, Western Australia, *Econ. Geol., 68*, 1089–1097, 1973.

Trendall, A. F., The Hamersley Basin, in *Iron-Formation: Facts and Problems*, edited by A. F. Trendall and R. C. Morris, pp. 69–129, Elsevier Sci., New York, 1983.

Trendall, A. F., and J. G. Blockley, The iron formations of the Precambrian Hamersley Group, Western Australia, *Bull. Geol. Surv. West. Aust., 119*, 366 pp., 1970.

Vanyo, J. P., and S. M. Awramik, Stromatolites and Earth-Sun-Moon dynamics, *Precambrian Res., 29*, 121–142, 1985.

Visser, M. J., Neap-spring cycles reflected in Holocene subtidal large-scale bedform deposits: A preliminary note, *Geology, 8*, 543–546, 1980.

von Brunn, V., and T. R. Mason, Siliciclastic-carbonate tidal deposits from the 3000 m.y. Pongola Supergroup, South Africa, *Sediment. Geol., 18*, 245–255, 1977.

Wahr, J. M., The Earth's rotation, *Ann. Rev. Earth Planet. Sci., 16*, 231–249, 1988.

Walker, J. C. G., and K. J. Zahnle, Lunar nodal tide and distance to the Moon during the Precambrian, *Nature, 320*, 600–602, 1986.

Walter, M. R. (Ed.), *Stromatolites*, 790 pp., Elsevier Sci., New York, 1976.

Watchorn, M. B., Fluvial and tidal sedimentation in the 3000 Ma Mozaan Basin, South Africa, *Precambrian Res., 13*, 27–42, 1980.

Webb, D. J., On the reduction in tidal dissipation produced by increases in the Earth's rotation rate and its effect on the long-term history of the Moon's orbit, in *Tidal Friction and the Earth's Rotation II*, edited by P. Brosche and J. Sünder-mann, pp. 210–221, Springer-Verlag, New York, 1982.

Wells, J. W., Coral growth and geochronometry, *Nature, 197*, 948–950, 1963.

Wells, J. W., Problems of annual and daily growth-rings in corals, in *Palaeogeophysics*, edited by S. K. Runcorn, pp. 3–9, Academic, San Diego, Calif., 1970.

Williams, G. E., Late Precambrian tidal rhythmites in South Australia and the history of the Earth's rotation, *J. Geol. Soc. London, 146*, 97–111, 1989a.

Williams, G. E., Precambrian tidal sedimentary cycles and Earth's paleorotation, *Eos Trans. AGU, 70*, 33 and 40–41, 1989b.

Williams, G. E., Tidal rhythmites: Geochronometers for the ancient Earth-Moon system, *Episodes, 12*, 162–171, 1989c.

Williams, G. E., Tidal rhythmites: Key to the history of the Earth's rotation and the lunar orbit, *J. Phys. Earth, 38*, 475–491, 1990.

Williams, G. E., Upper Proterozoic tidal rhythmites, South Australia: Sedimentary features, deposition, and implica-tions for the earth's paleorotation, in *Clastic Tidal Sedimen-tology*, edited by D. G. Smith et al., *Mem. Can. Soc. Pet. Geol., 16*, 161–177, 1991.

Williams, G. E., History of Earth's rotation and the Moon's orbit: A key datum from Precambrian tidal strata in Aus-tralia, *Aust. J. Astron., 5*, 135–147, 1994.

Williams, G. E., Precambrian length of day and the validity of tidal rhythmite paleotidal values, *Geophys. Res. Lett., 24*, 421–424, 1997.

Williams, G. E., Late Neoproterozoic periglacial aeolian sand sheet, Stuart Shelf, South Australia, *Aust. J. Earth Sci., 45*, 733–741, 1998a.

Williams, G. E., Precambrian tidal and glacial clastic deposits: Implications for Precambrian Earth-Moon dynamics and palaeoclimate, *Sediment. Geol., 120*, 55–74, 1998b.

Yoder, C. F., Astrometric and geodetic properties of Earth and the solar system, in *Global Earth Physics: A Handbook of Physical Constants*, edited by T. J. Ahrens, *AGU Ref. Shelf, 1*, 1–31, 1995.

G. E. Williams, Department of Geology and Geophysics, University of Adelaide, Adelaide, SA 5005, Australia. (george. williams@adelaide.edu.au)